Curling Probe Measurement in Plasma

Mr. Chatchai Sirithipvanich

จุฬาลงกรณ์มหาวิทยาลัย
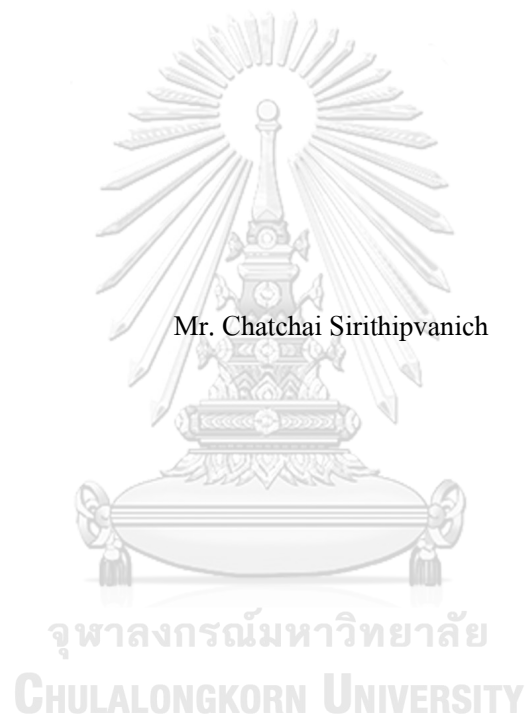CHULALONGKORN UNIVERSITY

A Thesis Submitted in Partial Fulfillment of the Requirements

for the Degree of Master of Science in Physics

Department of Physics

Faculty of Science

Chulalongkorn University

Academic Year 2019

หัววัดพลาสมาแบบขดเป็นวงก้นหอย

นายฉัตรชัย ศิริทิพย์วานิช

วิทยานิพนธ์นี้เป็นส่วนหนึ่งของการศึกษาตามหลักสูตรปริญญาวิทยาศาสตรมหาบัณฑิต
สาขาวิชาฟิสิกส์ ภาควิชาฟิสิกส์
คณะวิทยาศาสตร์ จุฬาลงกรณ์มหาวิทยาลัย
ปีการศึกษา 2562
ลิขสิทธิ์ของจุฬาลงกรณ์มหาวิทยาลัย

Thesis Title   Curling Probe Measurement in Plasma

By   Mr. Chatchai Sirithipvanich

Field of Study   Physics

Thesis Advisor   Assistant Professor BOONCHOAT PAOSAWATYANYONG,
                        Ph.D.

Accepted by the Faculty of Science, Chulalongkorn University in Partial Fulfillment of the Requirement for the Master of Science

.... Dean of the Faculty of Science
(Professor POLKIT SANGVANICH, Ph.D.)

THESIS COMMITTEE

.... Chairman
(Associate Professor SAKUNTAM SANORPIM, Ph.D.)

.... Thesis Advisor
(Assistant Professor BOONCHOAT PAOSAWATYANYONG, Ph.D.)

.... Examiner
(Associate Professor PIYABUT BURIKHaM, Ph.D.)

.... External Examiner
(Associate Professor Thawatchai Onjun, Ph.D.)

ฉัตรชัย ศิริทิพย์วานิช : หัววัดพลาสมาแบบขดเป็นวงก้นหอย. (Curling Probe Measurement in Plasma) อ.ที่ปรึกษาหลัก : ผศ. ดร.บุญโชติ เผ่าสวัสดิ์ยรรยง

หัววัดพลาสมาแบบขดเป็นวงก้นหอยเป็นหัววัดที่ทำงานด้วยวิธีการศึกษาสเปกตรัมการดูดซึมการสั่นพ้องแบบแอคทีฟ การศึกษาด้วยวิธีนี้ใช้สเปกตรัมของสัมประสิทธิ์การสะท้อนของหัววัดเพื่อวิเคราะห์หาความหนาแน่นของพลาสมา แบบจำลองสำหรับการวิเคราะห์หัววัดแบบขดเป็นวงก้นหอยที่ถูกเสนอ ใช้การเปลี่ยนแปลงของความถี่แมทช์ของหัววัด หรือความถี่ที่ซึ่งสัมประสิทธิ์การสะท้อนมีค่าต่ำที่สุด เมื่อหัววัดอยู่ในตัวกลางที่แตกต่างกัน โครงสร้างของหัววัดมีความเรียบง่าย และถูกอ้างโดยผู้เสนอหัววัดว่ามีความทนทานและมีประสิทธิภาพ คณะผู้วิจัยได้ทำการทดลองกับหัววัดที่คณะผู้วิจัยสร้างขึ้น และการจำลองผลเพื่อหาค่าสัมประสิทธิ์การสะท้อนของหัววัดแบบวงก้นหอยทั้งรูปแบบที่เคยถูกตีพิมพ์แล้ว และรูปแบบที่พวกเราสร้างขึ้นมา แบบจำลองที่ถูกเสนอไว้ก่อนหน้านี้ไม่สามารถใช้อธิบายผลการทดลองและการจำลองของคณะผู้วิจัยได้ อย่างไรก็ตามผลการทดลองและผลการจำลองของคณะผู้วิจัยสอดคล้องกัน และบ่งชี้ว่าความถี่แมทช์ไม่ตอบสนองต่อการเปลี่ยนแปลงของความหนาแน่นพลาสมา

สาขาวิชา ฟิสิกส์	ลายมือชื่อนิสิต ....
ปีการศึกษา 2562	ลายมือชื่อ อ.ที่ปรึกษาหลัก ....

5971928323 : MAJOR PHYSICS

KEYWORD: Curling Probe, Electromagnetic Field, Electrodynamics, Plasma, Plasma

Density, Plasma Diagnostics, Transmission Line, Reflection Coefficient

Chatchai Sirithipvanich : Curling Probe Measurement in Plasma. Advisor: Asst. Prof.

BOONCHOAT PAOSAWATYANYONG, Ph.D.

The curling probe is one of the active resonance absorption spectroscopic methods, the methods utilized the probe reflection coefficient spectrum to determine the plasma density. The proposed model of the curling probe uses the deviation of the most matched frequency, the frequency in which the minimum reflection coefficient occurs, when the probe is submerged in different mediums. The probe structure is simple and claimed to be robust and efficient. The experiments of a curling probe were performed and the simulations for the probe reflection coefficient for both previously reported probe and the constructed probe configuration have been conducted. The previously reported model could not describe our experimental and simulated results. However, our simulation and experiments conformed and indicated that the most matched frequency did not respond to the change of plasma density.

Field of Study:	Physics	Student's Signature ....
Academic Year:	2019	Advisor's Signature ....

ACKNOWLEDGEMENTS

TABLE OF CONTENTS

จุฬาลงกรณ์มหาวิทยาลัย

CHULALONGKORN UNIVERSITY

LIST OF FIGURES

4

LIST OF TABLES

จุฬาลงกรณ์มหาวิทยาลัย
CHULALONGKORN UNIVERSITY

I INTRODUCTION

The low-temperature plasma technologies have been constantly developing and now have a great number of applications. Without them, the development of microelectronics or surface modifications of advanced materials would not be possible [1]. In the last few decades, its applications have been broadened to the medication such as plasma treatments and biocompatible material fabrications [2]. To optimize and control conditions for the specific application, plasma parameters such as electron temperature and electron density must be determined [1].

The study of plasma parameter determination is called plasma diagnostics. There are various well-developed techniques such as Langmuir probes and optical emission spectroscopy (OES). However, those well-developed techniques also have their drawbacks. For example, the Langmuir probes, they work perfectly in low pressure direct current discharge and radio-frequency discharge, with the help of some modifications [3]. For them, to be used in higher pressure discharge, the more complicated model is needed and so far, have not been verified [3]. For the OES, the technique is almost flawless for the monoatomic gases [4], however, the model becomes much more complicated for the molecular gases [4]. In the past, only low-pressure plasma discharges are used in application thus most of the diagnostic techniques are developed for only the low-pressure plasma. Due to the development of atmospheric plasma discharge, the higher-pressure plasma diagnostics now become a major interest.

Active plasma resonance spectroscopy is another area of plasma diagnostic technique. It is the terminology for the probes which are composed of dielectric materials and conductors, such as microwave resonator probe [5-7], multipole resonance [8-10] or curling probe [11-13]. When the probes are inserted into plasma, we consider probe and plasma as a system of electrical networks. The voltage reflection coefficient spectrum is measured and analyzed into the plasma density [14]. The background theory for the higher pressure of the technique is relatively simpler than the conventional, however, it is developing and has not been verified yet [3, 4, 9, 14].

The curling probe is one of the active plasma resonance spectroscopic methods, it could be the most promising technique because of their durable and simple design. Basically, It is a metal cylinder filled with dielectric material with one end etched into a spiral slot antenna as shown in **Figure 1** [11].

(a)   *(b)*
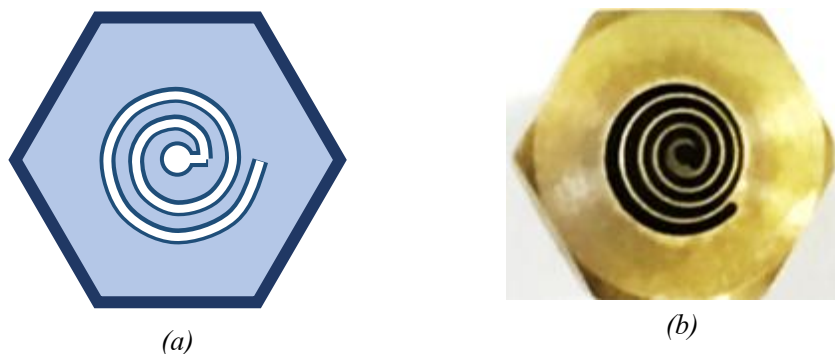
Figure 1 (a) the schematic of a spiral slot (b) the actual picture of spiral slot

1.1 OBJECTIVES

The aims of this thesis are constructing a curling probe, using the probe to measure plasma density and verifying its validity.

1.2 DEVELOPMENT OF THE CURLING PROBE

The curling probe is developed from the ideas of the microwave resonator probe and the hairpin probe by Liang, I. et al [11]. The development of the microwave resonator probe, hairpin probe, and curling probe will be presented. The microwave resonator probe is a U-shaped wire attached at the end of two coaxial transmission lines, it was developed for measuring the electron density in strongly magnetized plasma in 1976. The input signal was fed in one of the transmission lines, the signal was transmitted to the resonator via the coupling loop at the end of the line and the responses were picked up from the probe by another transmission line [5]. The schematics of the first microwave resonator designed by Stenzel, R. L. is shown in **Figure 2**. Stenzel constructed the probe and used it for measuring the electron density in the strongly magnetized plasma discharge. the probe was used along with other diagnostics tools including the Langmuir probe and whistler wave dispersion diagnostics. The electron density measurements using microwave resonator probe and whistler wave dispersion diagnostics agreed but the Langmuir probe results were not shown in the articles, the electron density results are shown in **Figure 3**.

0. 1 mm Ag WIRE

2 mm

INPUT

OUTPUT

$\lambda/4$

8 mm

f_{res} = 7.45 GHz

$Q \simeq 150$
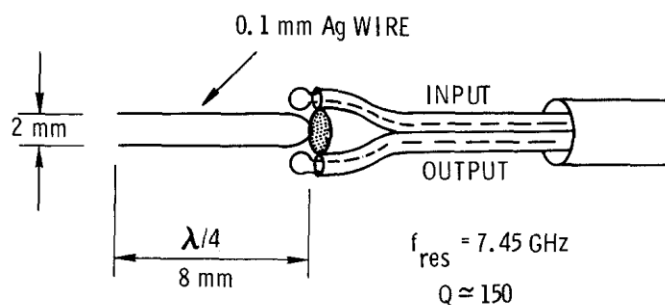
Figure 2 *The microwave resonator probe schematics proposed by Stenzel, R. L. [5]*
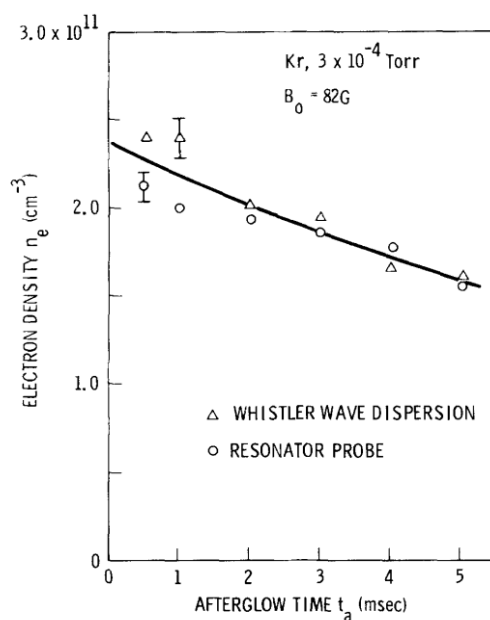
Figure 3 *The electron density measured by the microwave resonator probe and whistler wave*
dispersion diagnostics [5].

The microwave resonator probe was intensively verified and improved in 2004 by Piejak, R. B.,
et al. they reduced the probe dimensions by included the plasma sheath effect and also introduced
new configurations for microwave resonators using only a single coaxial transmission line. The
new configuration was called the reflection probe since the reflected responses were utilized
while the usual probe utilized the transmitted responses picked up by another transmission line
[7]. The modified probe was called the hairpin probe. The accuracy, precision, and reproducibility
of the hairpin probe were tested. The accuracy was tested by comparing between the hairpin
probe and the Langmuir probe electron density measurements in inductively coupled plasma. The

precision and reproducibility of the hairpin probe were excellence, while the comparison of plasma density measurements of the hairpin probe and Langmuir probe were different, but the trends of electron density measured by both probes were the same. The plasma density measurement range was mentioned to be between 10^{10} cm^{-3} and 10^{12} cm^{-3}. The comparison between hairpin and Langmuir probe measurements are shown in **Figure 4**.
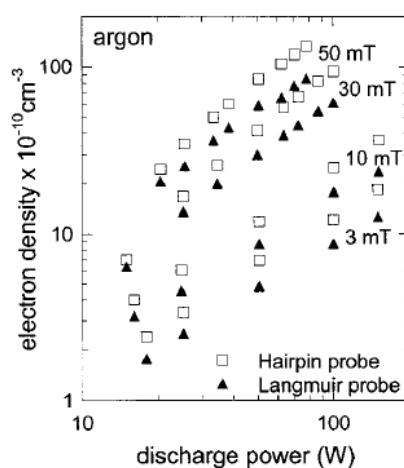
Figure 4 *The electron density measurements of the hairpin and Langmuir probe.*

The curling probe was developed by modifying the U-shaped wire of reflection hairpin probe into a narrow slot. The authors claimed that they are equivalent in terms of an antenna [11]. The probe model adopted the microwave resonator probe model modified by including geometrical and correction factors [11]. Those factors were added because the plasma density measurements were not actually performed but simulated using CST microwave studio. for the model to be a good fit with the simulated results the additional factors were needed. Both reflection hairpin probe and curling probe utilized the voltage reflection coefficient to determine the matched frequencies which will be interpreted as the resonance frequencies of the probe [7, 11]. Be noted that when the simulation is used, the independent variable is the plasma density not the matched frequencies. The schematics of curling probe is shown in **Figure 11** and the simulated voltage reflection coefficient and the relation between matched frequency and electron density are shown in **Figure 6**.

The model used for the microwave resonator probe is the same as the opened transmission line resonator model in transmission line theory which is presented in section 2.5 and the modification of microwave resonator probe model for the curling probe is presented in section 2.6.
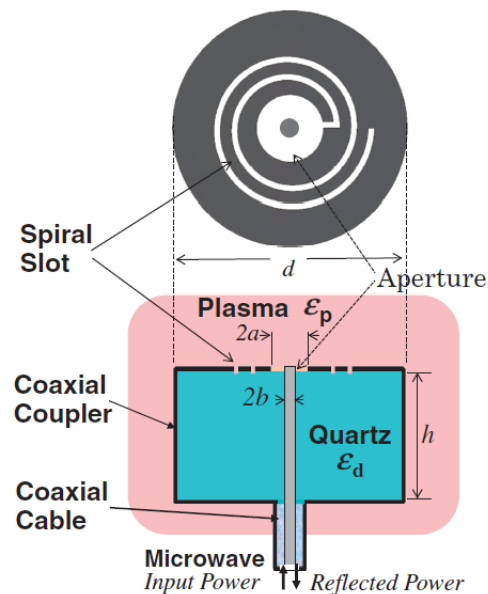
Figure 5 The curling probe schematic using in simulation model by Iji Liang, et al. [11]
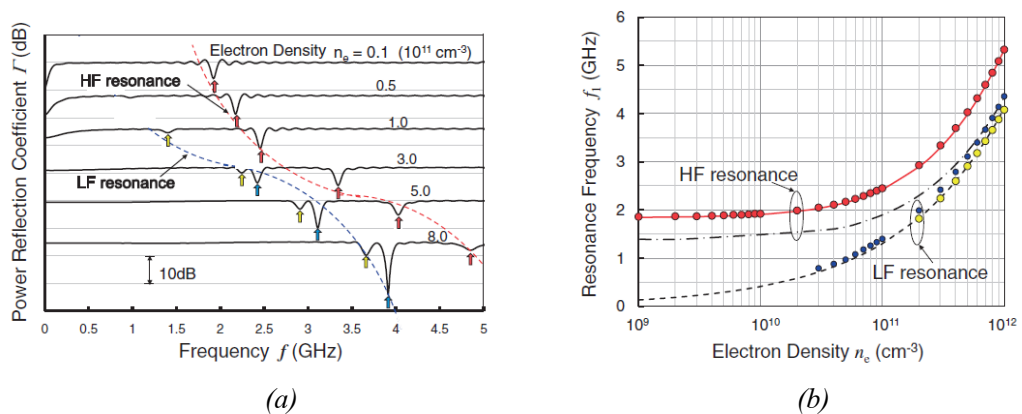
Figure 6 (a) The voltage reflection coefficient simulated in the curling probe article [11], (b) the matched frequency vs electron density.

II THEORETICAL BACKGROUND

The curling probe is formulated base on the wave characteristic of voltage and current, occurs in a transmission line. When we consider the whole system of a transmission line, for instant, the conductors and the dielectric between the conductors, the transmission line will grant 2 more properties, the characteristic impedance and the propagation constant. The characteristic impedance is defined because there will be current even if the transmission line is not terminated. The current would not produce work when the transmission line is lossless, the propagation constant indicates the attenuation and wavelength of the voltage wave along the transmission line. When the transmission line is biased with a sinusoidal voltage source, the voltage along the infinitely long transmission line behaves as a sinusoidal wave called the incident wave. If the transmission line is loaded, the voltage wave will be reflected by the load, the reflected voltage wave is called the reflected wave. The proportion of the reflected wave and incident wave is specified by the different of the load impedance and characteristic impedance of the transmission line. If the load impedance and characteristic impedance of the transmission line are identical, there will be no reflected wave and the load is said to be matched with the transmission line. Normally the load impedance is not constant over a range of frequency, thus when the load matches at a specific frequency, the frequency is called matched frequency. This chapter divided into 6 sections. The transmission line theory, the lossless transmission line, waveguide and connection between waveguide and transmission line will be present in the first 4 sections. The last 2 sections devoted to the curling probe model development. The first article which proposed the curling probe [11] models the curling probe as a transmission line resonator thus the theory of transmission line resonator is introduced first, and then the modeling of the curling probe as a transmission line resonator.

2.1 TRANSMISSION LINE THEORY

Assume that there is a transmission line lies along the z axis and the transmission line is modeled as a cascade series of lumped-element circuits with length dz in **Figure 7**. Let z indicates the position of lumped elements in the transmission line and the lumped elements consist of 4 components which are series resistor per unit length R , series inductor per unit length L, shunt conductance per unit length G and shunt capacitor per unit length C.
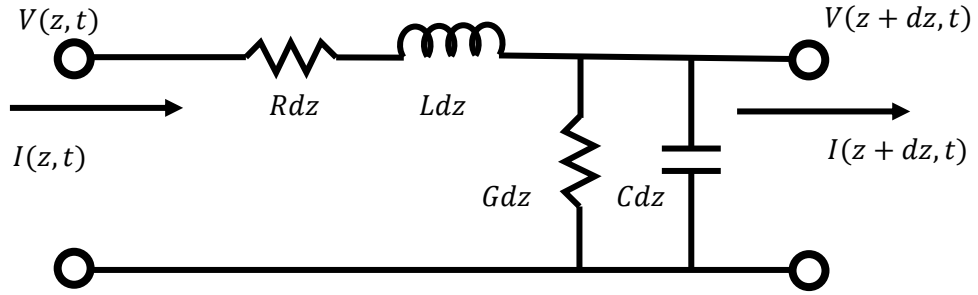
Figure *7 Lumped-element equivalent circuit of a transmission line section*

Define the voltage at the left and the right node as $V(z, t)$ and $V(z + dz, t)$ respectively, the current on the upper line enter the circuit as $I(z)$ and leave as $I(z + dz, t)$. Using both Kirchhoff's voltage and current laws, we get a system of transmission line differential equations

$$\frac{\partial V}{\partial z} = L\frac{\partial I}{\partial t} + RI \tag{1.1}$$

$$\frac{\partial I}{\partial z} = C\frac{\partial V}{\partial t} + GV \tag{1.2}$$

which lead to the differential equations of I and V

$$\left[\frac{\partial^2}{\partial z^2} - \left(L\frac{\partial}{\partial t} + R\right)\left(C\frac{\partial}{\partial t} + G\right)\right]\begin{bmatrix}V\\I\end{bmatrix} = 0$$

Assume time-dependent factor to be $\exp(-i\omega t)$, we have

$$\left[\frac{\partial^2}{\partial z^2} - (R - i\omega L)(G - i\omega C)\right]\begin{bmatrix}V\\I\end{bmatrix} = 0 \tag{2}$$

From equation (2), the time-independent solutions of the voltage and current in a transmission line are

$$V(z) = V_0^+ \exp(\gamma z) + V_0^- \exp(-\gamma z) \tag{3.1}$$

$$I(z) = I_0^+ \exp(\gamma z) + I_0^- \exp(-\gamma z) \tag{3.2}$$

Where γ is called the **complex propagation constant**

$$\gamma = \sqrt{(R - i\omega L)(G - i\omega C)} \tag{4}$$

According to the transmission line equation (1), when substitute voltage V with the solution equation (3), we get the current I in term of voltage V

$$I(z) = \frac{\gamma}{R - i\omega L}(V_0^+ \exp(\gamma z) - V_0^- \exp(-\gamma z)) \tag{5}$$

Define **characteristics impedance** Z_0 as

$$Z_0 = \frac{R - i\omega L}{\gamma} = \sqrt{\frac{R - i\omega L}{G - i\omega C}} \tag{6}$$

Consider the complex propagation constant as

$$\gamma = -\alpha + i\beta \tag{7}$$

The voltage and current in a transmission line will behave like attenuating waves with attenuating factor $\frac{1}{\alpha}$ and wavelength $\lambda = \frac{2\pi}{\beta}$.

2.2 LOSSLESS TRANSMISSION LINES AND LOAD EFFECT

The lossless transmission line is modeled without resistance R and conductance G per unit length, thus, the complex propagation constant and characteristics impedance are

$$\gamma = i\omega\sqrt{LC} \tag{8}$$

$$Z_0 = \sqrt{\frac{L}{C}} \tag{9}$$

Notice that, for a lossless transmission line $\alpha = 0$ and $\beta = \omega\sqrt{LC}$. We may represent a lossless transmission line as (Z_0, β)

When terminated a lossless transmission line with a load, consider the connection is made at $z = 0$ as in **Figure 8**. Using equations (3) and (5), the relationship between the load and the transmission line are

$$Z_L = \frac{V(0)}{I(0)}$$

$$Z_L = \frac{V_0^+ + V_0^-}{V_0^+ - V_0^-} Z_0 \tag{10}$$

$$\frac{V_0^-}{V_0^+} = \frac{Z_L - Z_0}{Z_L + Z_0} \tag{11}$$

and we define **the voltage reflection coefficient** as

$$\Gamma = \frac{V_0^-}{V_0^+} \tag{12}$$
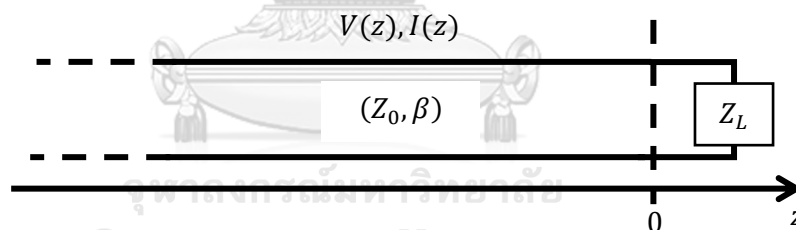
Figure 8 *A lossless transmission line terminated by a Z_L impedance load*

We introduce the voltage reflection coefficient because we sometimes cannot directly measure voltage and current as well as for high frequency, it is difficult to detect exact phases of the voltage and current at a specific point.

2.3 WAVEGUIDES

A waveguide is modeled as infinitely long hollow metallic cylinders. In the present discussion, the boundary metallic surfaces are assumed to be perfect conductors. We start from time-

independent Maxwell's equations in a homogeneous source-free medium for time-harmonic fields with time factor $\exp(-i\omega t)$.

$$\vec{\nabla} \cdot \vec{D} \quad = \quad 0 \tag{13.1}$$

$$\vec{\nabla} \cdot \vec{B} \quad = \quad 0 \tag{13.2}$$

$$\vec{\nabla} \times \vec{E} \quad = \quad i\omega\mu\vec{H} \tag{13.3}$$

$$\vec{\nabla} \times \vec{H} \quad = \quad -i\omega\epsilon\vec{E} \tag{13.4}$$

Taking curl on equations (13.3) and (13.4), we get the Helmholtz equation of electric and magnetic fields.

$$[\nabla^2 + \mu\epsilon\omega^2]\begin{bmatrix}\vec{E}\\\vec{H}\end{bmatrix} \quad = \quad 0 \tag{14}$$
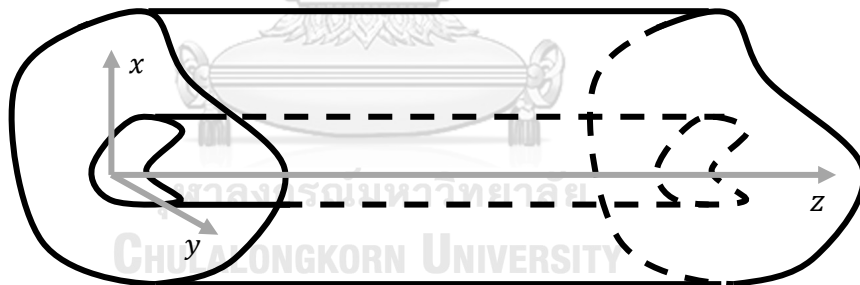
Figure 9 *Infinitely long hollow perfectly conducting cylinders*

Solving Helmholtz equations (14) with translation symmetry along z direction as in **Figure 9**. Rewrite the gradient operator separating the tangent and parallel to z components. We have

$$\vec{\nabla} \quad = \quad \vec{\nabla}_t + \hat{z}\frac{\partial}{\partial z} \tag{15}$$

where $\vec{\nabla}_t$ is the transverse 2-dimensional gradient. Then the solution will be

$$\vec{E}(x,y,z) \quad = \quad \vec{E}(x,y)\exp(\pm ik_z z) \tag{16.1}$$

$$\vec{H}(x,y,z) \quad = \quad \vec{H}(x,y)\exp(\pm ik_z z) \tag{16.2}$$

The Helmholtz equations are now turned into the 2-dimensional form

$$[\nabla_t^2 + (\omega^2 \mu \epsilon - k_z^2)]\begin{bmatrix}\vec{E}\\\vec{H}\end{bmatrix} \quad = \quad 0 \tag{17}$$

Separating vector fields into parallel and transverse to the propagating direction.

$$\vec{A} \quad = \quad \vec{A}_z + \vec{A}_t \tag{18.1}$$

$$\vec{A}_z \quad = \quad A_z \hat{z} \tag{18.2}$$

$$\vec{A}_t \quad = \quad \left(\hat{z} \times \vec{A}\right) \times \hat{z} \tag{18.3}$$

And then the time-independent Maxwell's equations (13) in an isotropic homogeneous medium can be written in term of parallel and transverse fields

$$\frac{\partial}{\partial z}\vec{E}_t + i\omega\mu\hat{z} \times \vec{H}_t \quad = \quad \vec{\nabla}_t E_z \tag{19.1}$$

$$\hat{z} \cdot \left(\vec{\nabla}_t \times \vec{E}_t\right) \quad = \quad i\omega\mu H_z \tag{19.2}$$

$$\frac{\partial}{\partial z}\vec{H}_t - i\omega\epsilon\hat{z} \times \vec{E}_t \quad = \quad \vec{\nabla}_t H_z \tag{19.3}$$

$$\hat{z} \cdot \left(\vec{\nabla}_t \times \vec{H}_t\right) \quad = \quad -i\omega\epsilon E_z \tag{19.4}$$

$$\vec{\nabla}_t \cdot \vec{E}_t \quad = \quad -\frac{\partial}{\partial z}E_z \tag{19.5}$$

$$\vec{\nabla}_t \cdot \vec{H}_t \quad = \quad -\frac{\partial}{\partial z}H_z \tag{19.6}$$

2.4 EQUIVALENT VOLTAGES AND CURRENTS FOR TEM SUPPORTED WAVEGUIDES

TEM supported waveguides need at least 2 separated conductors which will be labeled as positive and negative. For TEM wave, E_z and H_z are vanished, Maxwell's equations for TEM support waveguides are

$$\vec{\nabla}_t \cdot \vec{E}_t \quad = \quad 0 \tag{20.1}$$

$$\vec{\nabla}_t \cdot \vec{H}_t \quad = \quad 0 \tag{20.2}$$

$$\hat{z} \cdot \left(\vec{\nabla}_t \times \vec{E}_t \right) \quad = \quad 0 \tag{20.3}$$

$$\hat{z} \cdot \left(\vec{\nabla}_t \times \vec{H}_t \right) \quad = \quad 0 \tag{20.4}$$

$$\frac{\partial}{\partial z} \vec{E}_t + i\omega\mu\hat{z} \times \vec{H}_t \quad = \quad 0 \tag{20.5}$$

$$\frac{\partial}{\partial z} \vec{H}_t - i\omega\epsilon\hat{z} \times \vec{E}_t \quad = \quad 0 \tag{20.6}$$

The first 4 equations of (20) imply that potentials for transverse components of electric and magnetic fields can be defined. The last 2 equations give

$$\left[\frac{\partial^2}{\partial z^2} + \omega^2\mu\epsilon \right] \begin{bmatrix} \vec{E}_t \\ \vec{H}_t \end{bmatrix} \quad = \quad 0 \tag{21}$$

which implies that

$$k_z \quad = \quad \omega\sqrt{\mu\epsilon} \tag{22}$$

Voltage and current for a TEM waveguide are defined as

$$V_0 \quad = \quad \int_+^- \vec{E}_t \cdot d\vec{l} \tag{23.1}$$

$$I_0 \quad = \quad \oint_{C^+} \vec{H}_t \cdot d\vec{l} \tag{23.2}$$

where the integrating path for voltage is a simple curve connecting positive conductor and negative conductor while the integrating path for current is a positively oriented simple closed curve which enclosed the positive conductor, be noted that the integrating path is on the plane which perpendicular to the propagating direction. Even though $\vec{H}_t$ is irrotational, the domain is not simply connected so that the contour integration has not vanished. The characteristic impedance and complex propagation constant are

$$Z_0 \quad = \quad \sqrt{\frac{\mu}{\epsilon}} \left|\frac{V_0}{I_0}\right|^2 \frac{\int_S \vec{E}_t \cdot \vec{E}_t \, dS}{\int_S \vec{H}_t \cdot \vec{H}_t \, dS} \tag{24.1}$$

$$\gamma \quad = \quad i\omega\sqrt{\mu\epsilon} \tag{24.2}$$

Where S is the cross-sectional area of the transmission line medium. The TEM supported waveguide can now be modeled as a transmission line.

2.5 TRANSMISSION LINE RESONATORS

The length of a loaded transmission line can affect a load impedance. The transmission line resonator is a transmission line with finite length loaded with either open-circuited load or short-circuited load. Consider a transmission line with a finite length l loaded with Z_L as a single load.
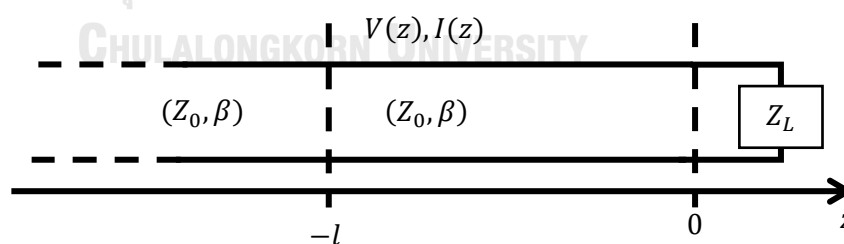
Figure 10 *The loaded transmission line with length l connected to a matched transmission line*

According to equations (3), (5), (10), (12), the impedance of the loaded transmission line with length l are

$$Z(-l) \quad = \quad \frac{V(-l)}{I(-l)}$$

$$\frac{V(-l)}{I(-l)} \quad = \quad Z_0 \left(\frac{\exp\left(-i\frac{2\pi}{\lambda}l\right) + \Gamma \exp\left(i\frac{2\pi}{\lambda}l\right)}{\exp\left(-i\frac{2\pi}{\lambda}l\right) - \Gamma \exp\left(i\frac{2\pi}{\lambda}l\right)} \right) \quad (25)$$

Where Γ is the reflection coefficient at $z = 0$

$$\Gamma \quad = \quad \frac{Z_L - Z_0}{Z_L + Z_0} \qquad (26)$$

consider resonator conditions, open-circuited and short-circuited loads.

For the open-circuited load, $|Z_L| \rightarrow \infty$ while the short-circuited load $Z_L = 0$. The reflection

coefficients for open-circuited and short-circuited loads are 1 and -1 respectively.

$$Z(-l)_{open} \quad = \quad -i \cot\left(\frac{2\pi}{\lambda}l\right) \qquad (27.1)$$

$$Z(-l)_{short} \quad = \quad i \tan\left(\frac{2\pi}{\lambda}l\right) \qquad (27.2)$$

Resonances occur when the impedance vanishes. The conditions for the open-circuited

transmission line resonators are $\frac{l}{\lambda} = \frac{1}{2}\left(n - \frac{1}{2}\right)$ when n is a positive integer, While the conditions

for the short-circuited transmission line resonators are $\frac{l}{\lambda} = \frac{n}{2}$ where n is a positive integer.

For a TEM open-circuited transmission line resonator, the resonance frequencies are

$$f \quad = \quad \frac{1}{2l}\left(n - \frac{1}{2}\right)\frac{1}{\sqrt{\mu\epsilon}} \qquad (28)$$

The first resonance frequency is

$$f \quad = \quad \frac{1}{4l}\frac{c}{\sqrt{\mu_r \epsilon_r}}$$

When the medium in the resonator is changed the resonance frequencies also change, consider the

ratio of the first resonance frequencies between vacuum and arbitrary medium.

$$\frac{f_0}{f} \quad = \quad \sqrt{\mu_r \epsilon_r} \qquad (29)$$

According to appendix A3, for a collisionless plasma $\mu_r = 1$ and $\epsilon_r = 1 - \frac{n_e e^2}{\epsilon_0 m_e (2\pi f)}$

$$\frac{f_0}{f} \quad = \quad \sqrt{1 - \left(\frac{n_e e^2}{2\pi \epsilon_0 m_e f}\right)^2}$$

Which can be used to find the plasma electron density

$$n_e \quad = \quad 2\pi \frac{\epsilon_0 m_e}{e^2} (f^2 - f_0^2) \qquad (30)$$

2.6 CURLING PROBE AS A TRANSMISSION LINE RESONATOR

A curling probe was first proposed in 2011 by Iji Liang, et al. [11]. using their simulated results, they claim that the spiral slot can be treated as a transmission line resonator connected to a coaxial transmission line as in **Figure 5** but the first resonance frequency is modified by assuming $\mu_r = 1$ and $\epsilon_{r,mod} = \frac{\epsilon_r + \epsilon_d}{2}$, the first resonance frequency becomes

$$f \quad = \quad \kappa \frac{c}{4l} \sqrt{\frac{2}{\epsilon_r + \epsilon_d}} \qquad (31)$$

Where ϵ_r is the relative permittivity of the medium which fills the slot, ϵ_d is the relative permittivity of the medium which fills the coaxial transmission line that supports the slot, κ is the geometrical correction factor and l is the length of the spiral slot. The plasma electron density is also derived from the ratio of the first resonance frequency when the slot is subject to the vacuum and plasma with additional correction factor δ.

$$n_e \quad = \quad \delta(1 + \epsilon_d) 2\pi \frac{\epsilon_0 m_e}{e^2} (f^2 - f_0^2) \qquad (32)$$

III METHODS AND RESULTS

To investigate the curling probes, we worked on both experiments and simulations. For the experiments, we had limitations on the size of our plasma chamber. we could not construct the probe mention in the first reported article [11] as it would too much disturb plasma. As we must keep the probe as small and simple as possible, we designed the probe from the female SMA-connector which the end cut into a spiral slot. For the simulations, we used commercial environment CST Microwave Studio, the same environment used to simulate the curling probe in the reported article, We tried to reproduce the result reported in the article [11] using the configuration mentioned in the article and also simulated our constructed probe configuration.

3.1 EXPERIMENTS

As we mentioned, we did not construct curling probes with the same specification as the previously reported design. The probe, we constructed, is much smaller. We machined a brass rod to construct a blank female SMA- connectors. Then, we drilled the end of the center. Finally, we wire-cut the end into a spiral slot as in **Figure 11**. The probes were not filled with quartz since pouring the molten quartz into brass mold would melt the mold.
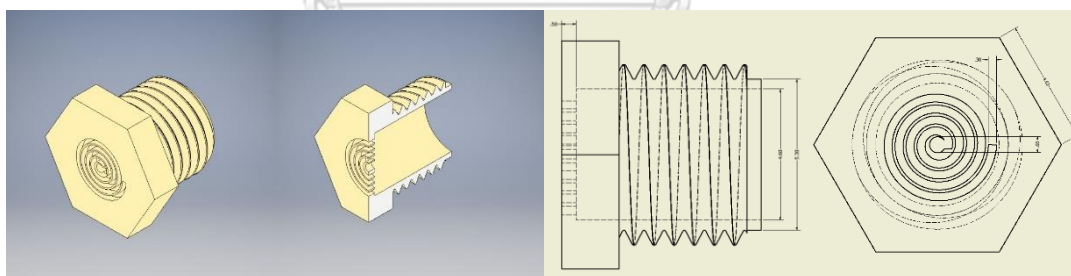
Figure 11 Schematics of a curling probe

The screw part of the path is the same as standard SMA, the end of the SMA is 0.5mm thick, the drilled center diameter is 0.6mm, the slot width is 0.3mm, and the spiral length is 35mm. The spiral length is the same as in the previously reported specification since it determined where to expected the resonance frequency [11]. The probe when properly coupled with the male SMA-connector is shown in **Figure 12**.
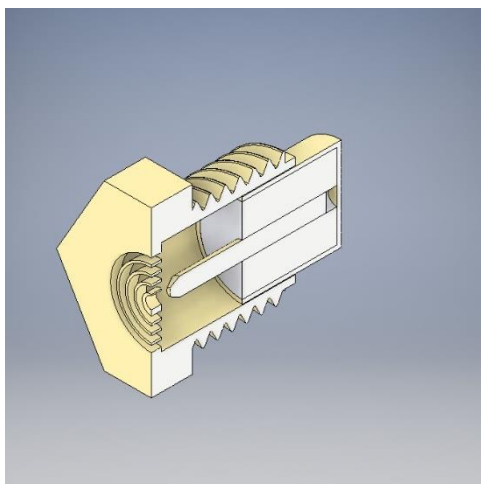
Figure 12 *Schematic of curling probe coupled with male SMA-connector*

The constructed probe's screw is too long to properly connect with male SMA-connector. The excess screw was shaved off to fit the male SMA-connector, as shown in Figure 13.

(a)   *(b)*
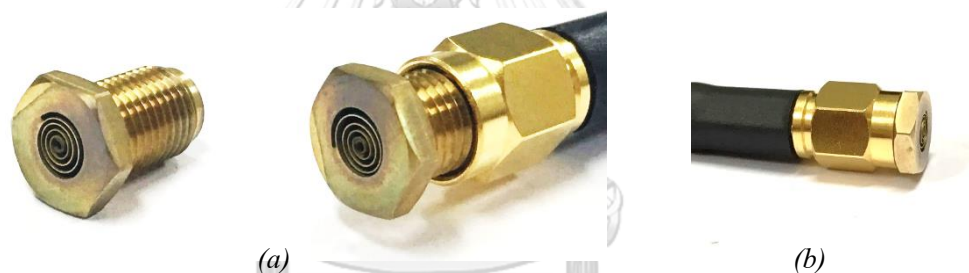
Figure 13 *(a) a constructed curling probe, (b) the curling probe shaved to fit a male SMA-connector*

3.1.1 EXPERIMENT SETUP

The experiments were performed using argon direct-current generated plasma. The plasma was generated in the vacuum chamber shown in **Figure 14**. The chamber was connected to Atlas Copco GVD3 rotary vacuum pump, capable of creating 10^{-3} mbar vacuum, and Aalborg GFC17 argon mass flow controller used to regulate argon gas flow to the chamber. The pressure in the chamber was measured by Edward API-100 active Pirani gauge, the absolute pressure gauge with a measurement range between 10^{-4} and 10^3 mbar.
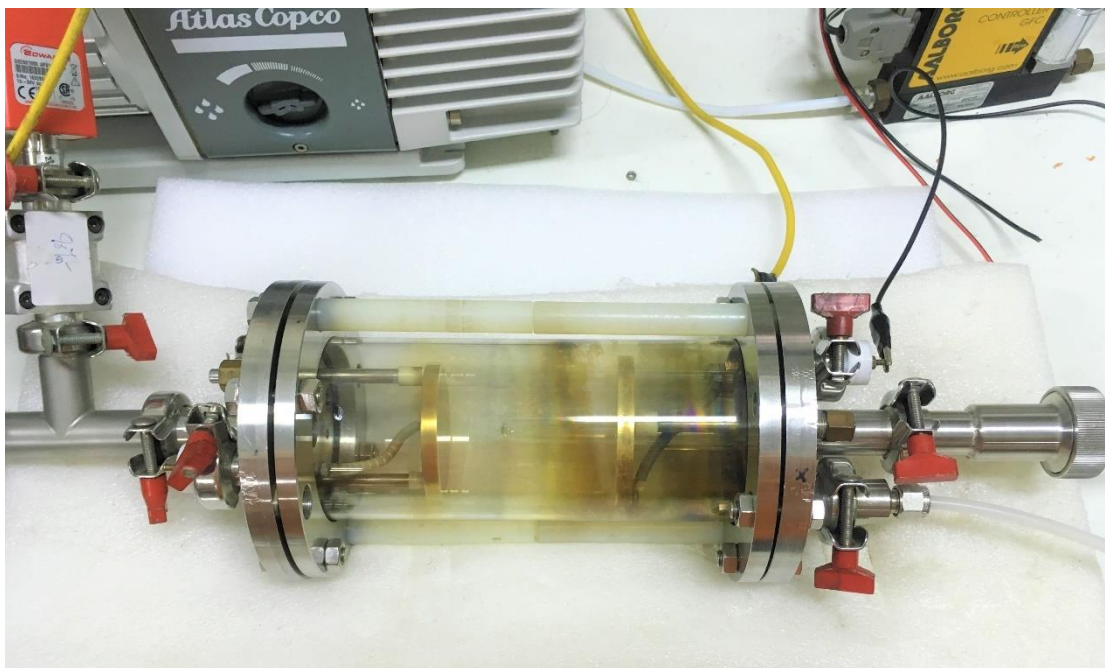
Figure 14 Plasma Chamber

The reflection coefficient of the curling probe is measured using Agilent E5071C Network
Analyzer with the measurement range of 9kHz to 8.5GHz. The RG142 coaxial cable is used to
connect the probe and the network analyzer. Because the network analyzer connection ports are
N-type connector, but the cable connectors are SMA, The N-type to SMA adaptor must be used.
The pictures of pressure gauge, mass flow controller, rotary vacuum pump, network analyzer,
adaptors, and cable are shown in **Figure 15**.

(a)   *(b)*   *(c)*

(d)   *(e)*   *(f)*
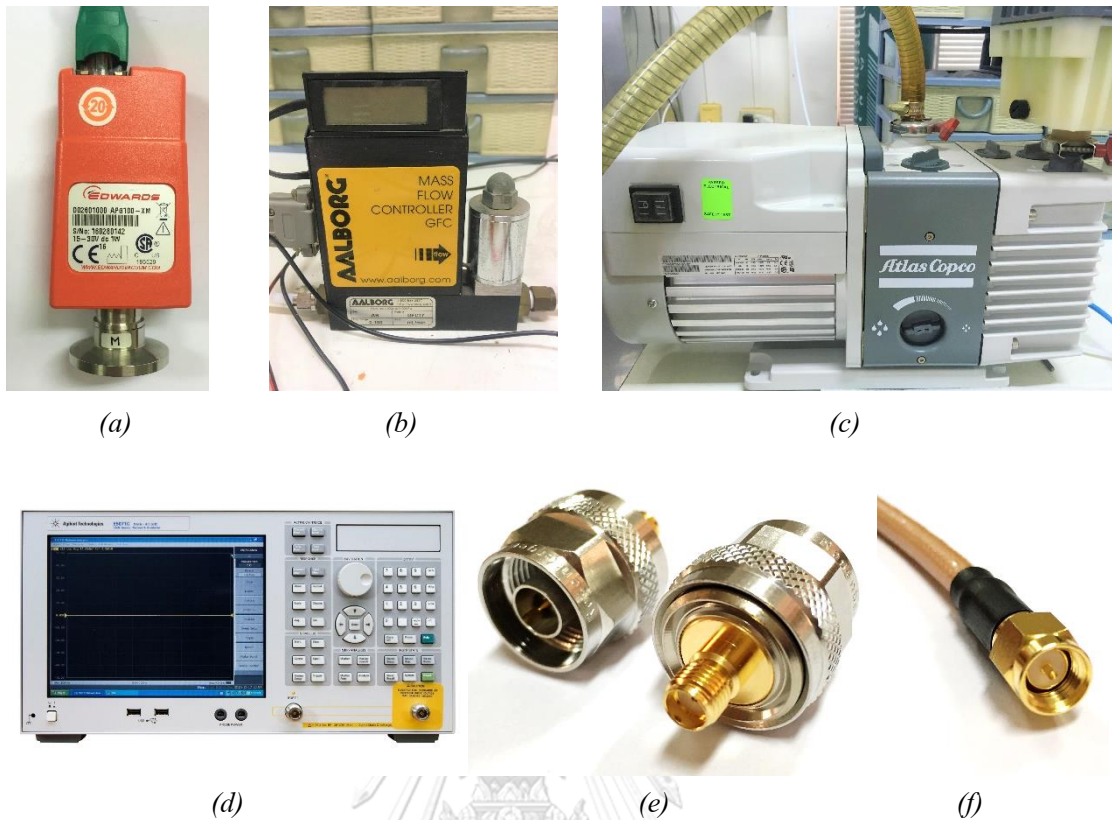
Figure 15 (a) Edward API-100 active Pirani gauge, (b) Aalborg GFC17 argon mass flow controller, (c) Atlas Copco GVD3 rotary vacuum pump, (e) Agilent E5071C Network Analyzer, (f) male N-type to female SMA Adaptors, (g) RG142 coaxial cable assembled with male SMA connectors on both ends.

The probe was protected by Pyrex tube, not directly exposed to the plasma as shown in **Figure 16**. The measurements of the reflection coefficient spectrum of the probe submerged in plasmas with 8 different conditions detailed in **Table 1**, the matched frequency occurred around 4.1956GHz and did not significantly change from experiment 1 where the plasma was not present as shown in **Figure 17**.

(a)

(b)   *(c)*
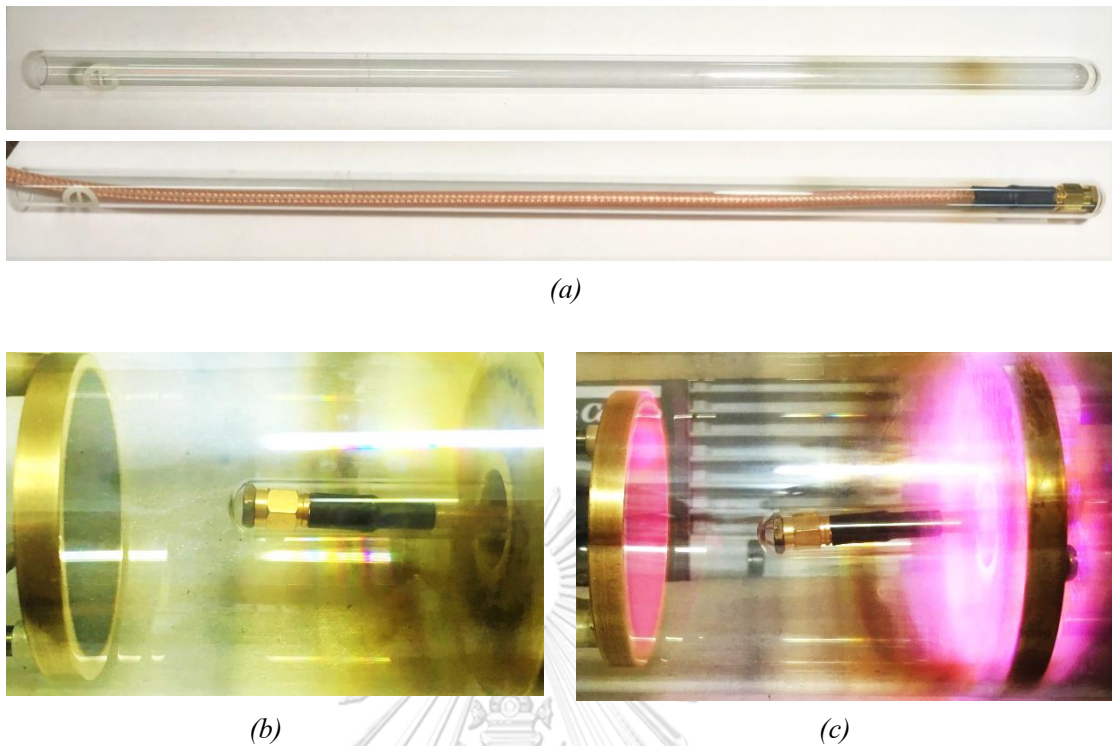
Figure 16 *(a) the Pyrex tube used to cover the curling probe and the curling probe, (b) The curling probe inside the plasma chamber, (c) The curling probe when plasma was generated.*

Experiment No.	Pressure (mbar)	Flow Rate (mL/min)	Volt (V)	Current (mA)	Power (W)	Matched Frequency (GHz)
1	0.55	40.0	0	0	0	4.1969
2	0.55	40.0	359	21	7.539	4.2022
3	0.55	40.0	430	61	26.230	4.1969
4	0.55	40.0	477	102	48.654	4.1916
5	0.65	50.5	316	12	3.792	4.1969
6	0.65	50.5	384	45	17.280	4.1969
7	0.65	50.5	422	81	34.182	4.1916
8	0.65	50.5	445	106	47.170	4.1916

Table 1 *The experimental results.*

To prepare the chamber conditions in **Table 1**, the chamber was vacuum until the pressure was 0.10 mbar and then the mass flow controller was turned on to pass the argon gas into the chamber, the flow rate was adjusted to get to the designated pressure.

(a)

(b)
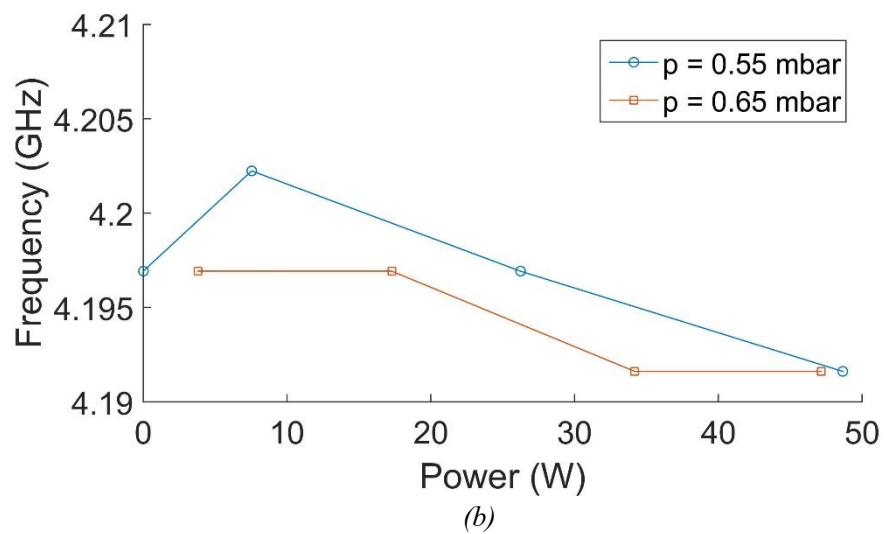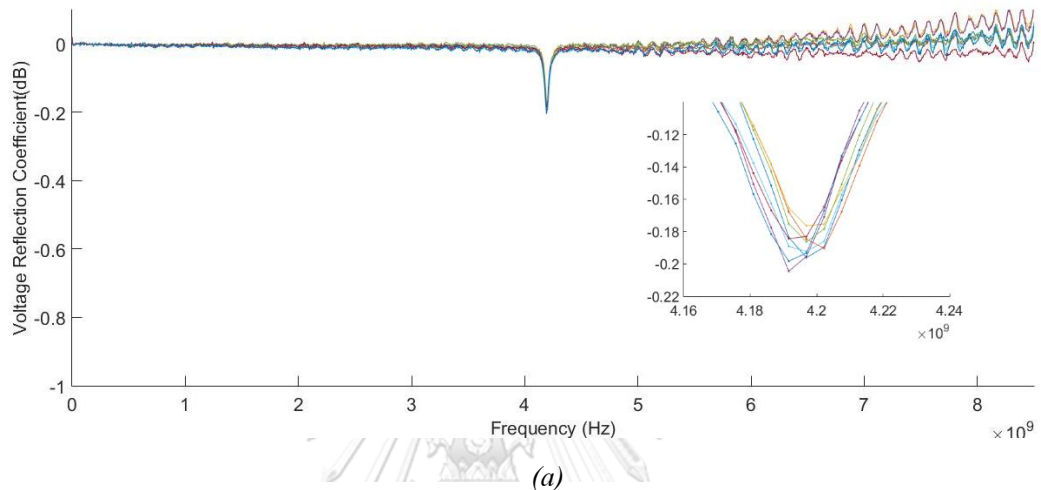
Figure 17 *(a) reflection coefficient spectrum of curling probe in plasmas, (b) the matched frequency where the reflection coefficient is minimum in each experiment.*

3.2 SIMULATIONS OF CURLING PROBE IN PLASMA

In the simulations, the CST microwave studio environment was used to simulate the reflection coefficient spectrum of 2 configurations of curling probes. The first configuration is the probe

proposed by the previously reported article and another configuration is close to our constructed

probe. The first configuration was chosen to directly compare the results to the previously

reported article [11] while the second configuration was chosen to compare with the constructed

probe in our experiments. The configurations used in the simulation are shown in **Figure 18** and

Figure 22.

The CST microwave studio environment is the commercial electrodynamic simulation software.

It is commonly used for solving Maxwell's equations with complex geometry boundary to

determine the measurable quantities, such as voltage reflection coefficient spectrum or radiation

profile. It is optimized for accuracy and low runtime and widely accepted by engineers.

3.2.1 CONFIGURATION 1 THE PREVIOUSLY REPORTED PROBE

Configuration 1 is the configuration specified in the previously reported probe. The probe is filled

with the dielectric which is quartz. the pre-defined quartz in the CST environment has relative

permittivity equal to 3.75 while the relative permittivity used in the article was 3.78. We used

Adobe Inventor to create a disk with spiral slot and build-in modeling tools of CST microwave

studio to create the rest of the probe. The probe was connected to a standard RG142 of length

7.5mm where a waveguided port was placed to the other end, as in **Figure 18**. The simulations

were performed in the time domain, by generating the input pulse which is the sum of the

interested spectrum of electromagnetic waves, using this method, the simulation of different

frequencies can be done at once. The simulation environment automatically generated the input

signal to match the coaxial transmission line mode. The criteria required for simulation to stop are

that the electromagnetic wave has dissipated, or that the simulation time has exceeded 200 times

of the input pulse duration. If the electromagnetic wave does not fully dissipate, the truncation

error will occur which causing ripples in reflection coefficient results [15]. An example of the

input and response signals of a low truncation error simulation is shown in **Figure 19**.
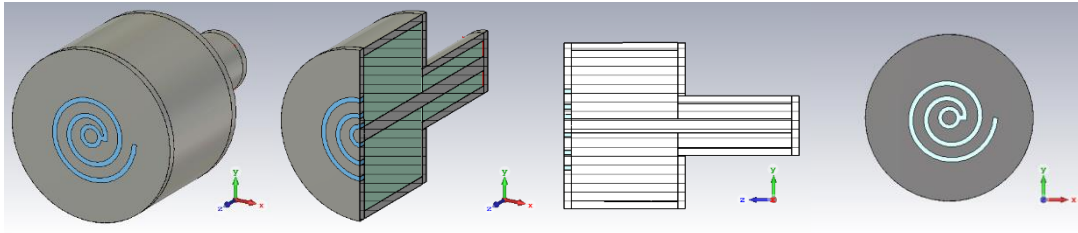
Figure 18 *The configuration used in simulations of the curling probe mentioned in [11]*

The early and late simulated input and output signals are shown in **Figure 19**, notice that the late output amplitude is at least 1000 times lower than the early output signal.
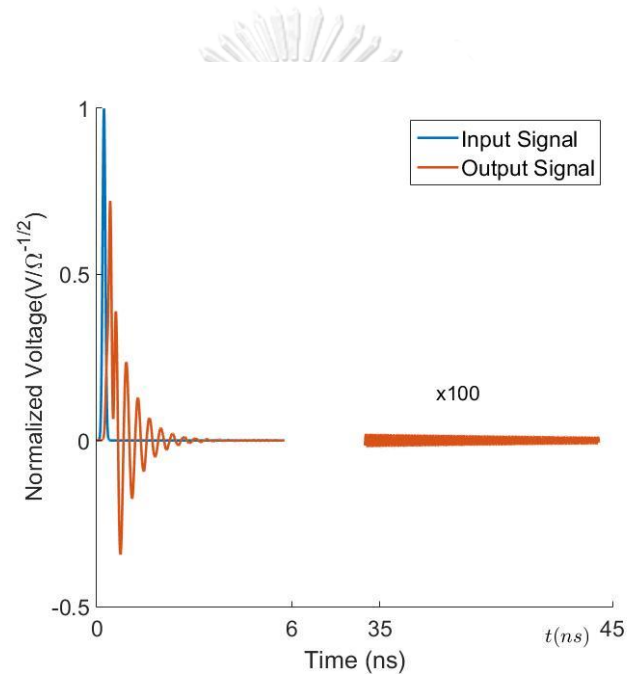
Figure 19 *Partial simulated input and output signals provided at the waveguide port.*

The simulated reflection coefficient spectrum of the previously reported probe [11] when the probe was in a vacuum and plasma are shown in **Figure 20**. The simulations are performed for plasma with various electron densities from 0.1×10^{11} to 100×10^{11} m^{-3}, the reflection coefficient results are closed to those shown in **Figure 20**.
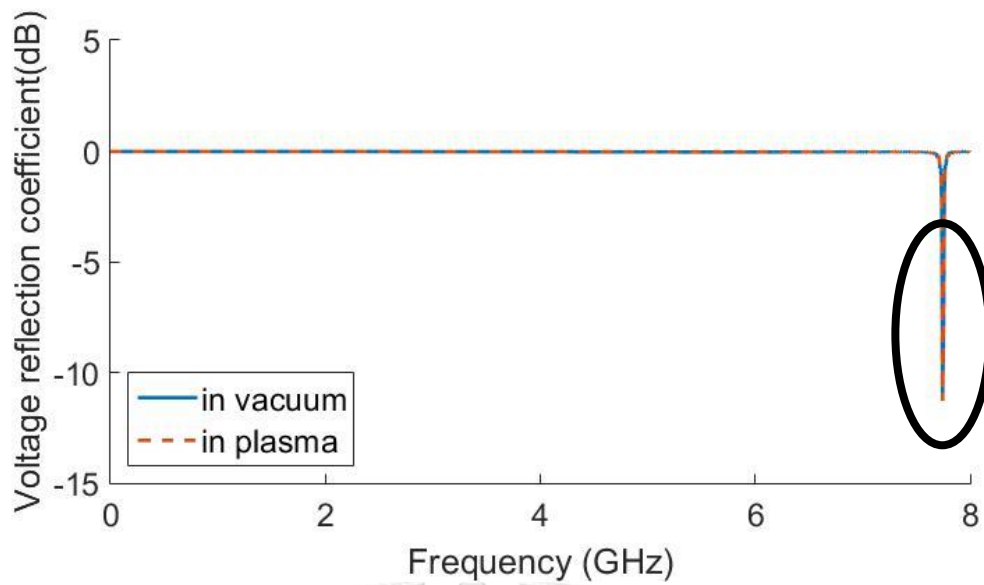
Figure 20 *the reflection coefficient spectrum from the simulation*

The only difference in reflection coefficient spectrums among simulations is the magnitude. The minimum occurred at the same frequency 7.744GHz. These results do not agree with the previously reported work [11].
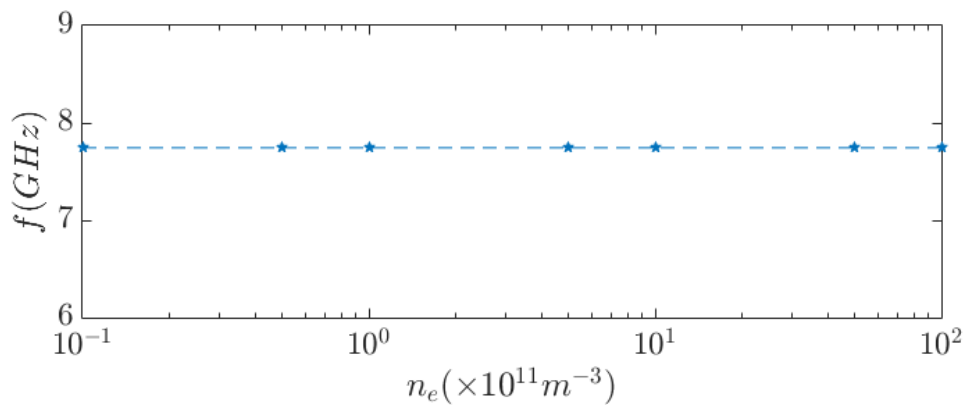
Figure 21 *the relation between minimum reflection coefficient frequency and plasma electron density from the simulated results*

3.2.2 CONFIGURATION 2 THE CONSTRUCTED PROBE

Configuration 2 is our constructed probe model used the same specification mentioned in the experiments section. Adobe Inventor and CST microwave studio build-in modeling tools are also used for modeling the probe. The coaxial line length is 7mm, 0.5mm shorter than the previous

model. The model is not the same as the experimental ones in section 3.1. The inner conductor of the probe is modified to fit the center hole at the end of the probe. The model is shown in **Figure 22**.
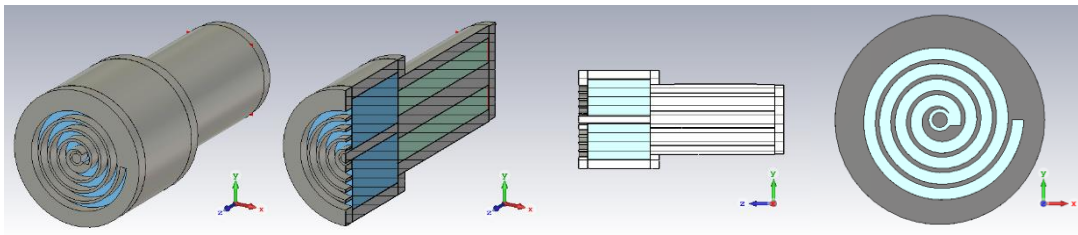
Figure 22 The model used to simulate the constructed probe.

The simulations stop when the output signal vanished or the simulated time reached 100 times of the input signal pulse. **Figure 23** shows the partial input and output signal at the early and late simulated time.
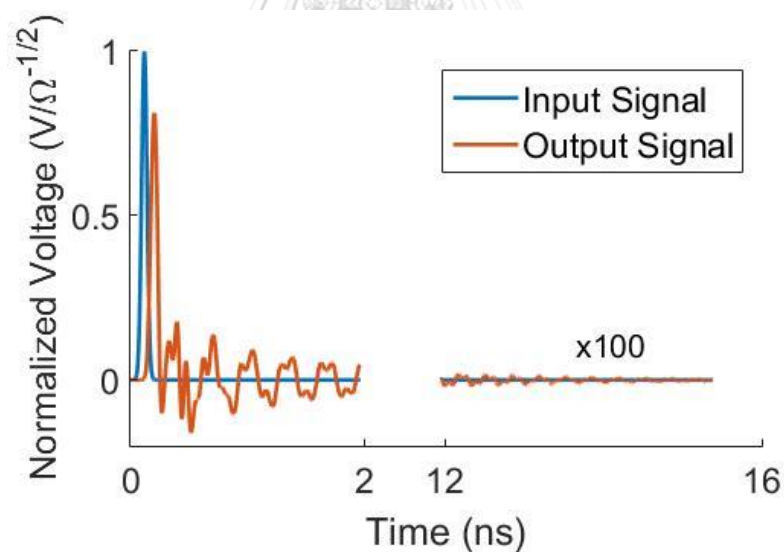
Figure 23 The simulate input and output signals provided to the waveguide port

The reflection coefficient results show 2 local minimums, the first local minimum magnitude is very low around 50mdB at 3.095GHz, while the second minimum is much greater in magnitude at 8.955GHz. **Figure 24** shows the reflection coefficients of the constructed probe in a vacuum

31

and a plasma. The simulations were performed in various electron densities range from 0.2×10^{11} to 100×10^{11} m^{-3}.
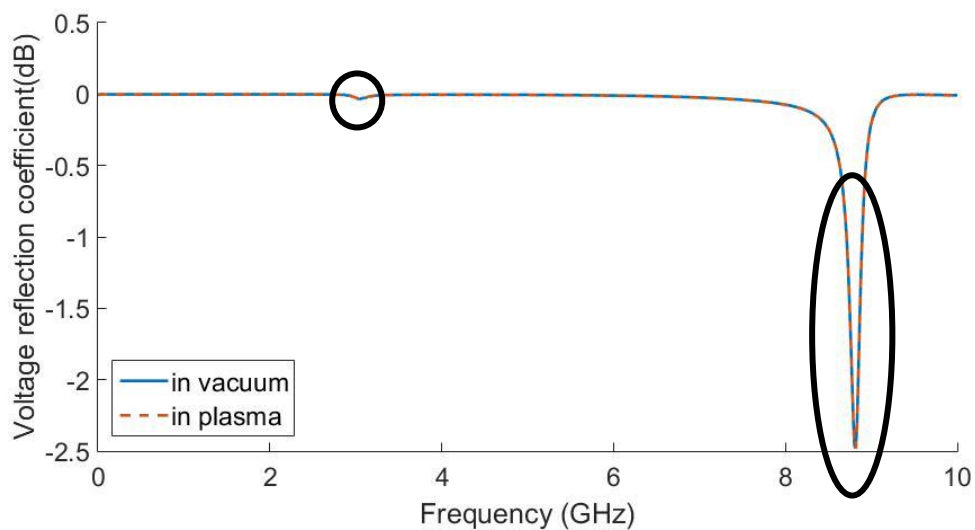
Figure 24 *the reflection coefficient spectrum from the simulation*

The frequencies, where both local minimums occur, did not shift when the electron density was changed as shown in **Figure 25**.
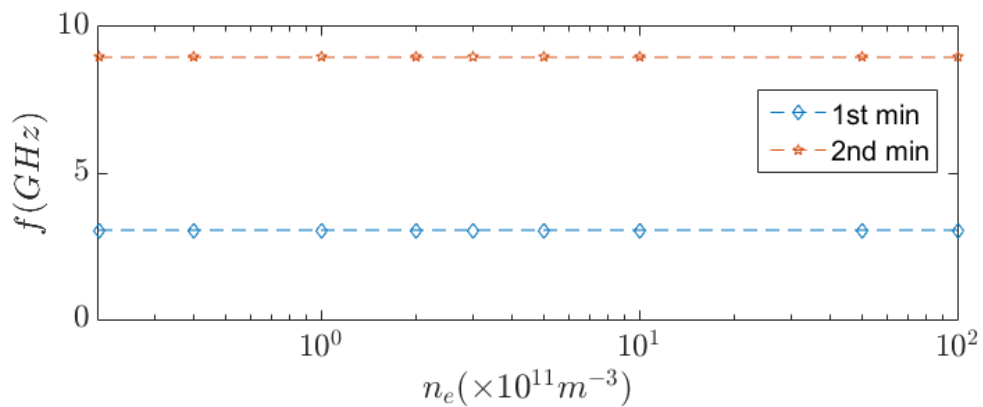
Figure 25 *the relation between minimum reflection coefficient frequencies and plasma electron density from the simulated results*

IV DISCUSSIONS AND FURTHER INVESTIGATION

The experiments of the constructed curling probe immerse in plasma with different densities do not indicate any significant shift of the curling probe matched frequency up to the maximum range of our network analyzer. The simulations also confirmed that the matched frequency of curling probes does not shift when plasma densities change. Our experiments and simulations cannot be described by the model reported in the previous article [11] which was using the simulation results to show that the matched frequency was shifting when the plasma frequency changed. To find the reasons why the probe could not detect the plasma density, we remodeled the probes from different basics, investigate in the probe responses and the probe's slot effect.

The remodeling motivated by the misconception of resonance frequency and matched frequency in the microwave resonator probe and its variations [7, 10, 11, 14]. They implied that when the load or, in this case, the probe were matched, it was also resonant which is not true. The resonance is, as mention in section 2.5, when the load impedances vanishes or infinitely large while the load is said to be matched when the load impedance is equal to the characteristic impedance of transmission line. According to the flaw, the transmission line is extremely necessary when the voltage reflection coefficient spectrum is one of the measurable in the model. The previously proposed model excluded the transmission line implicitly. The ideas for our analysis motivated by Arshadi's work [16]. Instead of using vector potentials, we used the fields themselves directly. The vector potential analysis attained electromagnetic fields in the forms that cannot analytically analyze for the reflection coefficient spectrum and the analysis is overly complicated since, we must map known properties of the electromagnetic fields, such as the orthogonality and boundary conditions into the vector potential space. The result of the investigation is presented from section 4.1 to 4.3 The model based on the single slit model which will be completely constructed in section 4.2. The single slit model is applied for the curling probe problem to estimate the voltage reflection coefficient spectrum in section 4.3.

Even though the probe voltage reflection coefficient spectrum did not respond to the change of plasma density, the spectrum responded to the presence of other material. We investigated the behavior of the probe on this matter by experiments and simulations in section 4.4.

To ensure that the minimum in the voltage reflection coefficient spectrum was not the results of the slot on the probe face, we simulated the voltage reflection coefficient spectrum when the probe was

covered with the perfectly conducting disk and when the probe face was replaced by the perfectly conducting disk in section 4.5.

The results of our model predicted the minimum in the voltage reflection coefficient spectrum. However, when the probe was in contact with non-dispersive material, the minimum did not occur. The predictions also suggest that the matched frequency should respond to the change of plasma density. This contradicted the results in both section 3.1 and section 4.4. the model cannot be used to describe the system.

According to the results in section 4.4, the curling probe can sense the material which was placed in front of it in the range from 0mm to approximately 3mm. The matched frequency when the probe directly contacts the materials was inversely proportional to the relative permittivity, but the assumption cannot be implied since the thickness of each material were not controlled. If the assumption were true, it cannot be implied for the plasma case since the plasma is a dispersive medium.

We first hypothesized that the voltage reflection coefficient spectrum does not respond to the change of plasma density because the plasma information lost through the thickness of the slot or the signal itself excited by the slot but not the medium in front of it. The hypotheses were contradicted by the results in sections 4.4 and 4.5, the information of mediums can be sensed by the probe. Unfortunately, the mediums do not include the plasma, the slot itself without a medium in front of it did not excite the minimum in the voltage reflection coefficient spectrum. The slot can also pass the medium information.

In the experiments in plasma section 3.1, the probe was covered by a Pyrex tube, this may be the reason why the probe cannot detect the plasma presence. Unfortunately, we cannot directly expose the probe in the plasma. When the probe directly exposed in the plasma, the plasma arcing between an electrode and the probe occurs and This phenomenon discharged a relatively large amount of current into the probe. We cannot ensure that our measurement tools can handle the phenomenon, the experiment of the probe exposed directly to the plasma cannot be performed.

4.1 COMPLETE SOLUTION OF THE HELMHOLTZ'S EQUATION

The standard Helmholtz's equations take form

$$(\nabla^2 + k^2)\phi \quad = \quad 0 \tag{33}$$

The solutions are

$$\phi_{k_x,k_y,k_z}(x,y,z) \quad = \quad \phi_{0_{k_x,k_y,k_z}} \exp\big(i(k_x x + k_y y + k_z z)\big)$$

where k_x, k_y, k_z are complex numbers and satisfy

$$k^2 \quad = \quad k_x^2 + k_y^2 + k_z^2$$

Define wave vector

$$\vec{k} \quad = \quad (k_x, k_y, k_z)$$

Where

$$\vec{k} \cdot \vec{k} \quad = \quad k^2$$

The degree of freedom of choosing a wave vector is 2. We can choose 2 out of 3 elements of the wave vector. Conventionally k_x and k_y are chosen, Then

$$k_z \quad = \quad \sqrt{k^2 - k_x^2 - k_y^2}$$

The integrations of all possible solutions [17] are

$$\phi^{\pm}(x,y,z) \quad = \quad \int_{-\infty}^{\infty} \int_{-\infty}^{\infty} \tilde{\phi}(k_x, k_y) \exp\left(i(k_x x + k_y y \pm k_z z)\right) dk_x \, dk_y$$

Where the superscript $+$ and $-$ signs indicate the outgoing and incoming waves in z-direction respectively. For the sake of simplicity, we considered the cases where k_y is 0 or the 2-dimensional problems which reduces the degree of freedom into 1.

$$\phi^{\pm}(x,z) = \int_{-\infty}^{\infty} \tilde{\phi}(k_x) \exp\big(i(k_x x \pm k_z z)\big) \, dk_x \qquad (34.1)$$

$$k_z = \sqrt{k^2 - k_x^2} \qquad (34.2)$$

The integrations of all possible solutions are called the spectrum of plane waves.

4.2 THE ELECTROMAGNETIC WAVES IN PIECEWISE HOMOGENEOUS MEDIUM WITH PLANE INTERFACE

Define piecewise homogeneous medium as the 2 or more homogeneous mediums with different permittivity and permeability in contact with each other. The surface where 2 homogeneous mediums contacts will be called interface between the mediums. In our problem, we were solving the electromagnetic waves in 2 homogeneous mediums in contact with the plane interface. The complete solution of plane waves will be applied to the boundary condition problem of piecewise homogeneous medium with the plane interface. The results when only a wave vector is considered [18] are recovered from the model. The effects of a thin slit, modeled as the thin perfectly conducting plane, that is placed at the interface can now be investigated.

We will find that for the normal incident, the reflection and transmission coefficient does not affect by the slit, they have the same form as the piecewise homogeneous medium. We then used the reflection and transmission coefficient of the slit model to estimate the voltage reflection coefficient spectrum of the curling probe in the next section.

4.2.1 PIECEWISE HOMOGENEOUS MEDIUM

The piecewise homogeneous medium with a plane interface is defined by piecewise constant permittivity and permeability, the medium is defined as

$$\epsilon(x,y,z) \quad = \quad \begin{cases} \epsilon_1 & z < 0 \\ \epsilon_2 & z \geq 0 \end{cases} \tag{35.1}$$

$$\mu(x,y,z) \quad = \quad \begin{cases} \mu_1 & z < 0 \\ \mu_2 & z \geq 0 \end{cases} \tag{35.2}$$

In this case, the interface is the xy-plane.
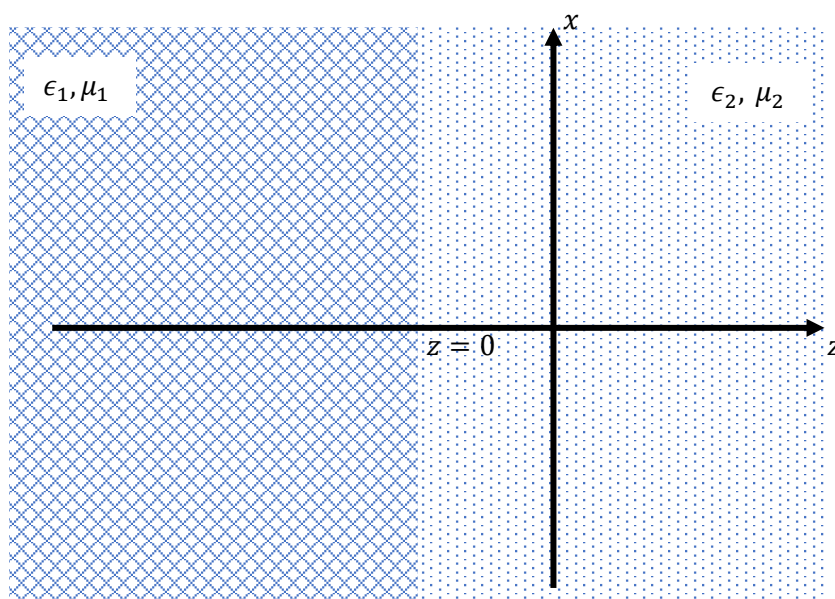
Figure 26 *The piecewise homogenous medium with plane discontinuity*

Recall Maxwell's equations (13) and the electromagnetic wave equations (14)

$$\vec{\nabla} \cdot \vec{D} \quad = \quad 0$$

$$\vec{\nabla} \cdot \vec{B} \quad = \quad 0$$

$$\vec{\nabla} \times \vec{E} \quad = \quad i\omega\mu\vec{H}$$

$$\vec{\nabla} \times \vec{H} \quad = \quad -i\omega\epsilon\vec{E}$$

$$[\nabla^2 + \mu\epsilon\omega^2]\begin{bmatrix} \vec{E} \\ \vec{H} \end{bmatrix} \quad = \quad 0$$

The wave equation implies that

$$E_{x^i}(x, y, z) \quad = \quad \tilde{E}^{\pm}_{0x^i} \exp\left(i\left(k_x x + k_y y \pm k_z z\right)\right) \tag{36}$$

where $x^i \in \{x, y, z\}$, lead to

$$\vec{\nabla} \times \vec{E} \quad = \quad i\vec{k} \times \vec{E}$$

$$\vec{H} \quad = \quad \sqrt{\frac{\epsilon}{\mu}} \hat{k} \times \vec{E} \tag{37}$$

Resulting in the orthogonality among the electric field, magnetic field, and wave vector.

$$\vec{k} \cdot \begin{bmatrix} \vec{E} \\ \vec{H} \end{bmatrix} \quad = \quad 0$$

$$\vec{E} \cdot \vec{H} \quad = \quad 0$$

Meaning that the electric field, magnetic field and wave vector are perpendicular to each other. The field solutions (36) work almost everywhere in the previously defined piecewise homogeneous medium (35) but at $z = 0$. Since the solutions in $z < 0$ and $z > 0$ are different, those solution will be linked at $z = 0$ according to Maxwell's equations

$$\left(\vec{D}_1 - \vec{D}_2\right) \cdot \hat{n} \quad = \quad 0 \tag{38.1}$$

$$\left(\vec{B}_1 - \vec{B}_2\right) \cdot \hat{n} \quad = \quad 0 \tag{38.2}$$

$$\left(\vec{E}_1 - \vec{E}_2\right) \times \hat{n} \quad = \quad 0 \tag{38.3}$$

$$\left(\vec{H}_1 - \vec{H}_2\right) \times \hat{n} \quad = \quad 0 \tag{38.4}$$

where $\hat{n}$ is the vector normal to xy-plane. In order to get simple analytic results, we will analyze the problem in 2-dimension. Assuming we know there is an incident wave propagating in the positive z-direction, once the incident wave approaches the discontinuity there will be reflected wave propagating back into negative z-direction or $z < 0$ and transmitted wave propagating into positive z-direction or $z > 0$. Define xy-plane normal vector

$$\hat{n} \quad = \quad (0,0,1) \tag{39}$$

wave vectors for the incident, reflect and transmitted waves

$$\vec{k}^i \quad = \quad \left(k_x, 0, \sqrt{k_1^2 - k_x^2}\right) \tag{40.1}$$

$$\vec{k}^r \quad = \quad \left(k_x, 0, -\sqrt{k_1^2 - k_x^2}\right) \tag{40.2}$$

$$\vec{k}^t \quad = \quad \left(k_x, 0, \sqrt{k_2 - k_x^2}\right) \tag{40.3}$$

where $k_1 = \omega\sqrt{\epsilon_1\mu_1}$ and $k_2 = \omega\sqrt{\epsilon_2\mu_2}$. The solution of electric fields for this problem is the complete 2-dimensional Helmholtz solution together with orthogonality between electric field and wave vectors, electric fields of the incident, reflected, and transmitted waves are

$$\vec{E}^i(x,z) \quad = \quad \int_{-\infty}^{\infty} \vec{E}_0^i(k_x^i) \exp\left(i(k_x x + k_z^i z)\right) dk_x^i$$

$$\vec{E}^r(x,z) \quad = \quad \int_{-\infty}^{\infty} \vec{E}_0^r(k_x^r) \exp\left(i(k_x^r x + k_z^r z)\right) dk_x^r$$

$$\vec{E}^t(x,z) \quad = \quad \int_{-\infty}^{\infty} \vec{E}_0^t(k_x^t) \exp\left(i(k_x^t x + k_z^t z)\right) dk_x^t$$

Where the vector kernels without exponential factor $\tilde{E}_0^i(k_x^i), \tilde{E}_0^r(k_x^r)$ and $\tilde{E}_0^t(k_x^t)$ are

$$\vec{E}_0^i(k_x) \quad = \quad \left(\tilde{E}_{0xz}^i(k_x^i)\frac{k_z^i}{k_1}, \tilde{E}_{0y}^i(k_x^i), -\tilde{E}_{0xz}^i(k_x^i)\frac{k_x^i}{k_1}\right) \tag{41.1}$$

$$\vec{E}_0^r(k_x) \quad = \quad \left(-\tilde{E}_{0xz}^r(k_x^r)\frac{k_z^r}{k_1}, \tilde{E}_{0y}^r(k_x^r), \tilde{E}_{0xz}^r(k_x^r)\frac{k_x^r}{k_1}\right) \tag{41.2}$$

$$\vec{E}_0^t(k_x) \quad = \quad \left(\tilde{E}_{0xz}^t(k_x^t)\frac{k_z^t}{k_2}, \tilde{E}_{0y}^t(k_x^t), -\tilde{E}_{0xz}^t(k_x^t)\frac{k_x^t}{k_2}\right) \tag{41.3}$$

For the electric displacement fields, the magnetic fields, and the magnetic inductions. The only difference from the electric fields is the kernel without the exponential factor. The following definition will focus on kernels. The electric displacement field kernels

$$\vec{D}_0^i(k_x) \quad = \quad \epsilon_1\left(\tilde{E}_{0xz}^i(k_x^i)\frac{k_z^i}{k_1}, \tilde{E}_{0y}^i(k_x^i), \tilde{E}_{0xz}^i(k_x^i)\frac{k_x^i}{k_1}\right) \quad (42.1)$$

$$\vec{D}_0^r(k_x) \quad = \quad \epsilon_1\left(\tilde{E}_{0xz}^r(k_x^r)\frac{k_z^r}{k_1}, \tilde{E}_{0y}^r(k_x^r), \tilde{E}_{0xz}^r(k_x^r)\frac{k_x^r}{k_1}\right) \quad (42.2)$$

$$\vec{D}_0^t(k_x) \quad = \quad \epsilon_2\left(\tilde{E}_{0xz}^t(k_x^t)\frac{k_z^t}{k_2}, \tilde{E}_{0y}^t(k_x^t), \tilde{E}_{0xz}^t(k_x^t)\frac{k_x^t}{k_2}\right) \quad (42.3)$$

The magnetic field kernels

$$\vec{H}_0^i(k_x) \quad = \quad \sqrt{\frac{\epsilon_1}{\mu_1}}\hat{k}^i \times \left(\tilde{E}_{0xz}^i(k_x^i)\frac{k_z^i}{k_1}, \tilde{E}_{0y}^i(k_x^i), \tilde{E}_{0xz}^i(k_x^i)\frac{k_x^i}{k_1}\right) \quad (43.1)$$

$$\vec{H}_0^r(k_x) \quad = \quad \sqrt{\frac{\epsilon_1}{\mu_1}}\hat{k}^r \times \left(\tilde{E}_{0xz}^r(k_x^r)\frac{k_z^r}{k_1}, \tilde{E}_{0y}^r(k_x^r), \tilde{E}_{0xz}^r(k_x^r)\frac{k_x^r}{k_1}\right) \quad (43.2)$$

$$\vec{H}_0^t(k_x) \quad = \quad \sqrt{\frac{\epsilon_2}{\mu_2}}\hat{k}^t \times \left(\tilde{E}_{0xz}^t(k_x^t)\frac{k_z^t}{k_2}, \tilde{E}_{0y}^t(k_x^t), \tilde{E}_{0xz}^t(k_x^t)\frac{k_x^t}{k_2}\right) \quad (43.3)$$

The magnetic induction kernels

$$\vec{B}_0^i(k_x) \quad = \quad \sqrt{\epsilon_1\mu_1}\hat{k}^i \times \left(\tilde{E}_{0xz}^i(k_x^i)\frac{k_z^i}{k_1}, \tilde{E}_{0y}^i(k_x^i), \tilde{E}_{0xz}^i(k_x^i)\frac{k_x^i}{k_1}\right) \quad (44.1)$$

$$\vec{B}_0^r(k_x) \quad = \quad \sqrt{\epsilon_1\mu_1}\hat{k}^r \times \left(\tilde{E}_{0xz}^r(k_x^r)\frac{k_z^r}{k_1}, \tilde{E}_{0y}^r(k_x^r), \tilde{E}_{0xz}^r(k_x^r)\frac{k_x^r}{k_1}\right) \quad (44.2)$$

$$\vec{B}_0^t(k_x) \quad = \quad \sqrt{\epsilon_2\mu_2}\hat{k}^t \times \left(\tilde{E}_{0xz}^t(k_x^t)\frac{k_z^t}{k_2}, \tilde{E}_{0y}^t(k_x^t), \tilde{E}_{0xz}^t(k_x^t)\frac{k_x^t}{k_2}\right) \quad (44.3)$$

Since we have already known the incident wave meaning that $\tilde{E}_{0xz}^i$ and $\tilde{E}_{0y}^i$ are known, there are only 4 unknowns left which are $\tilde{E}_{0xz}^r$, $\tilde{E}_{0xz}^t$, $\tilde{E}_{0y}^r$ and $\tilde{E}_{0y}^t$. The boundary conditions (38) consist of 6 equations, this means the systems are over constraint or they are repeated.

$$D_{1z} - D_{2z} \quad = \quad 0$$

$$B_{1z} - B_{2z} \quad = \quad 0$$

$$E_{1y} - E_{2y} \quad = \quad 0$$

$$E_{1x} - E_{2x} \quad = \quad 0$$

$$H_{1y} - H_{2y} \qquad = \qquad 0$$

$$H_{1x} - H_{2x} \qquad = \qquad 0$$

At $z = 0$, boundary conditions (38) when substituting subscripted 1 fields with the superposition of incident and reflected fields and subscripted 2 fields with transmitted fields, we get

$$\int_{-\infty}^{\infty} \left(\epsilon_2 \frac{k_x}{k_2} \tilde{E}_{0xz}^t - \epsilon_1 \frac{k_x}{k_1} \left(\tilde{E}_{0xz}^r - \tilde{E}_{0xz}^i \right) \right) \exp(ik_x x) \, dk_x \qquad = \quad 0 \quad (45.1)$$

$$\int_{-\infty}^{\infty} \left(\sqrt{\epsilon_1 \mu_1} \frac{k_x}{k_1} \left(\tilde{E}_{0y}^r + \tilde{E}_{0y}^i \right) - \sqrt{\epsilon_2 \mu_2} \frac{k_x}{k_2} \tilde{E}_{0y}^t \right) \exp(ik_x x) \, dk_x \qquad = \quad 0 \quad (45.2)$$

$$\int_{-\infty}^{\infty} \left(\tilde{E}_{0y}^r + \tilde{E}_{0y}^i - \tilde{E}_{0y}^t \right) \exp(ik_x x) \, dk_x \qquad = \quad 0 \quad (45.3)$$

$$\int_{-\infty}^{\infty} \left(\frac{\sqrt{k_2^2 - k_x^2}}{k_2} \tilde{E}_{0xz}^t - \frac{\sqrt{k_1^2 - k_x^2}}{k_1} \left(\tilde{E}_{0xz}^r + \tilde{E}_{0xz}^i \right) \right) \exp(ik_x x) \, dk_x \qquad = \quad 0 \quad (45.4)$$

$$\int_{-\infty}^{\infty} \left(\sqrt{\frac{\epsilon_1}{\mu_1}} \left(-\tilde{E}_{0xz}^r + \tilde{E}_{0xz}^i \right) - \sqrt{\frac{\epsilon_2}{\mu_2}} \tilde{E}_{0xz}^t \right) \exp(ik_x x) \, dk_x \qquad = \quad 0 \quad (45.5)$$

$$\int_{-\infty}^{\infty} \left(\frac{\sqrt{k_1^2 - k_x^2}}{k_1} \sqrt{\frac{\epsilon_1}{\mu_1}} \left(\tilde{E}_{0y}^i - \tilde{E}_{0y}^r \right) - \frac{\sqrt{k_2^2 - k_x^2}}{k_2} \sqrt{\frac{\epsilon_2}{\mu_2}} \tilde{E}_{0y}^t \right) \exp(ik_x x) \, dk_x \quad = \quad 0 \quad (45.6)$$

Using the fact that $k_1 = \omega\sqrt{\epsilon_1 \mu_1}$ and $k_2 = \omega\sqrt{\epsilon_2 \mu_2}$ equation (45.2) recovers (45.3) and equation (45.1) recovers (45.5). Be reminded that $\tilde{E}_{0xz}^i$, $\tilde{E}_{0xz}^r$, $\tilde{E}_{0xz}^t$, $\tilde{E}_{0y}^i$, $\tilde{E}_{0y}^r$ and $\tilde{E}_{0y}^t$ are all functions of k_x. Consider only essential 4 equations regardless of how repeated equations are chosen, the results will be the same. In this case, we choose (45.3), (45.4), (45.5) and (45.6) of boundary conditions (45), we have

$$-\tilde{E}_{0y}^r + \tilde{E}_{0y}^t \quad = \quad \tilde{E}_{0y}^i \qquad (46.1)$$

$$-\frac{\sqrt{k_1^2 - k_x^2}}{k_1} \tilde{E}_{0xz}^r + \frac{\sqrt{k_2^2 - k_x^2}}{k_2} \tilde{E}_{0xz}^t \quad = \quad \frac{\sqrt{k_1^2 - k_x^2}}{k_1} \tilde{E}_{0xz}^i \qquad (46.2)$$

$$\sqrt{\frac{\epsilon_1}{\mu_1}} \tilde{E}_{0xz}^r + \sqrt{\frac{\epsilon_2}{\mu_2}} \tilde{E}_{0xz}^t \quad = \quad \sqrt{\frac{\epsilon_1}{\mu_1}} \tilde{E}_{0xz}^i \qquad (46.3)$$

$$\frac{\sqrt{k_1^2 - k_x^2}}{k_1} \sqrt{\frac{\epsilon_1}{\mu_1}} \tilde{E}_{0y}^r + \frac{\sqrt{k_2^2 - k_x^2}}{k_2} \sqrt{\frac{\epsilon_2}{\mu_2}} \tilde{E}_{0y}^t \quad = \quad \frac{\sqrt{k_1^2 - k_x^2}}{k_1} \sqrt{\frac{\epsilon_1}{\mu_1}} \tilde{E}_{0y}^i \qquad (46.4)$$

which can be solved for $\tilde{E}_{0xz}^r$, $\tilde{E}_{0xz}^t$, $\tilde{E}_{0y}^r$ and $\tilde{E}_{0y}^t$.

$$\tilde{E}_{0xz}^r(k_x) = \tilde{E}_{0xz}^i(k_x)\left[\frac{\sqrt{k_2^2 - k_x^2} - \frac{\epsilon_2}{\epsilon_1}\sqrt{k_1^2 - k_x^2}}{\sqrt{k_2^2 - k_x^2} + \frac{\epsilon_2}{\epsilon_1}\sqrt{k_1^2 - k_x^2}}\right] \quad (47.1)$$

$$\tilde{E}_{0xz}^t(k_x) = \tilde{E}_{0xz}^i(k_x)\left[\frac{2\sqrt{\frac{\epsilon_2\mu_2}{\epsilon_1\mu_1}}\sqrt{k_1^2 - k_x^2}}{\sqrt{k_2^2 - k_x^2} + \frac{\epsilon_2}{\epsilon_1}\sqrt{k_1^2 - k_x^2}}\right] \quad (47.2)$$

$$\tilde{E}_{0y}^r(k_x) = \tilde{E}_{0y}^i(k_x)\left[\frac{-\sqrt{k_2^2 - k_x^2} + \frac{\mu_2}{\mu_1}\sqrt{k_1^2 - k_x^2}}{\sqrt{k_2^2 - k_x^2} + \frac{\mu_2}{\mu_1}\sqrt{k_1^2 - k_x^2}}\right] \quad (47.3)$$

$$\tilde{E}_{0y}^t(k_x) = \tilde{E}_{0y}^i(k_x)\left[\frac{2\frac{\mu_2}{\mu_1}\sqrt{k_1^2 - k_x^2}}{\sqrt{k_2^2 - k_x^2} + \frac{\mu_2}{\mu_1}\sqrt{k_1^2 - k_x^2}}\right] \quad (47.4)$$

To realize the conventional solutions of a single wave vector case [18] we use the incident wave as

$$\vec{k}_0 = \left(k_{x0}, 0, \sqrt{k_1^2 - k_{x0}^2}\right) \quad (48.1)$$

$$\vec{\tilde{E}}_0^i(k_x) = \vec{\tilde{e}}_0^i \delta(k_x - k_{x0}) \quad (49.2)$$

where $\vec{\tilde{e}}_0^i$ is constant vector

$$\vec{e}_0^i = \left(\tilde{e}_{0xz}^i \frac{\sqrt{k_1^2 - k_{x0}^2}}{k_1}, \tilde{e}_{0y}^i, \tilde{e}_{0xz}^i \frac{k_{x0}}{k_1}\right)$$

This incident wave will recover the reflected and refracted wave amplitudes from the oblique incident wave to the plane interface between 2 mediums [18].

4.2.2 PIECEWISE HOMOGENEOUS MEDIUM WITH SLIT

Instead of leaving the mediums in contact with each other at the interface, a perfectly conducting plane that is cut in the middle is placed on the interface $z = 0$ as in **Figure 27**. The conducting plane is considered to be a slit. The boundary conditions (45) are valid when $|x| < l$ where there

is no conducting plane at the interface. But, when $|x| \geq l$ the superposition of incident and reflecting electric fields and transmitted electric field vanish.

$$\vec{E}^r(x,0) + \vec{E}^i(x,0) \quad = \quad 0 \tag{50.1}$$

$$\vec{E}^t(x,0) \quad = \quad 0 \tag{50.2}$$

Combination of (47) and (50) gives us a complete of $\vec{E}^r$ and $\vec{E}^t$ at $z = 0$.

$$\vec{E}^r(x,0) \quad = \quad \begin{cases} \vec{E}^i(x,0) & |x| \geq l \\ \int_{-\infty}^{\infty} \vec{\tilde{E}}_0^r(k_x) \exp(ik_x x)\, dk_x & |x| < l \end{cases} \tag{51.1}$$

$$\vec{E}^t(x,0) \quad = \quad \begin{cases} 0 & |x| \geq l \\ \int_{-\infty}^{\infty} \vec{\tilde{E}}_0^t(k_x) \exp(ik_x x)\, dk_x & |x| < l \end{cases} \tag{51.2}$$

Assuming the incident wave is a single wave vector wave (49), the scattered waves (51) become

$$\vec{E}^r(x,0) \quad = \quad \begin{cases} \vec{e}_0^i & |x| \geq l \\ \vec{\tilde{E}}_0^r(k_{x0}) & |x| < l \end{cases} \tag{52.1}$$

$$\vec{E}^t(x,0) \quad = \quad \begin{cases} 0 & |x| \geq l \\ \vec{\tilde{E}}_0^t(k_{x0}) & |x| < l \end{cases} \tag{52.2}$$

where $\vec{\tilde{E}}_0^r(k_{x0})$ and $\vec{\tilde{E}}_0^t(k_{x0})$

$$\vec{\tilde{E}}_0^r(k_{x0}) \quad = \quad \left(\tilde{E}_{0xz}^r(k_{x0}) \frac{\sqrt{k_1^2 - k_{x0}^2}}{k_1}, \tilde{E}_{0y}^r(k_{x0}), -\tilde{E}_{0xz}^r(k_{x0}) \frac{k_{x0}}{k_1} \right)$$

$$\vec{\tilde{E}}_0^t(k_{x0}) \quad = \quad \left(-\tilde{E}_{0xz}^t(k_{x0}) \frac{\sqrt{k_2^2 - k_{x0}^2}}{k_2}, \tilde{E}_{0y}^t(k_{x0}), \tilde{E}_{0xz}^t(k_{x0}) \frac{k_{x0}}{k_2} \right)$$

$\tilde{E}_{0xz}^r(k_{x0}), \tilde{E}_{0y}^r(k_{x0}), \tilde{E}_{0xz}^t(k_{x0})$ and $\tilde{E}_{0y}^t(k_{x0})$ can be found from (47) and (49) and suggest that $\vec{\tilde{E}}_0^r(k_{x0})$ and $\vec{\tilde{E}}_0^t(k_{x0})$ are constant vectors.
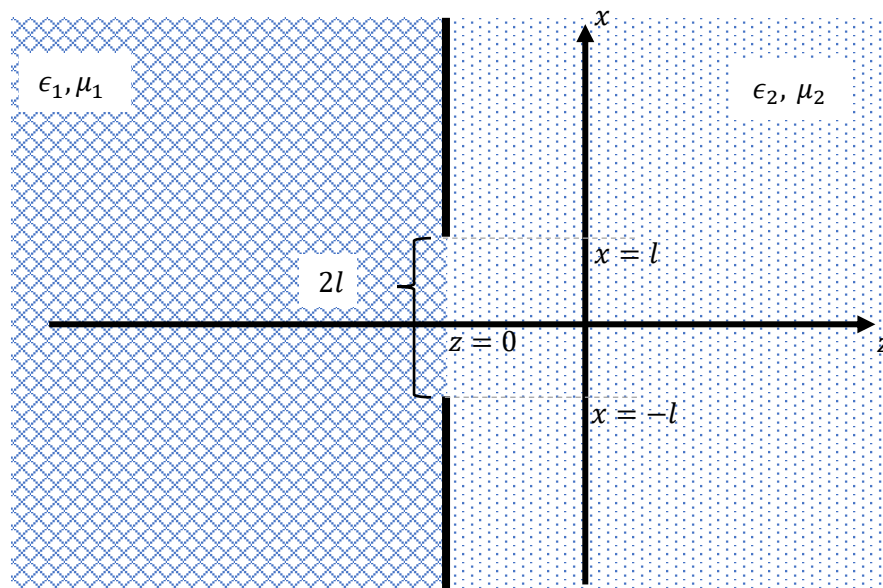
Figure 27 *The interface between dielectric is blocked with a perfectly conducting plane which the middle is cut into a slit of width* $2l$

Boundary conditions (46.1) and (46.2) gives us more insight relation among incident and scattered waves

$$\tilde{E}^r_{0y} = -\tilde{E}^i_{0y} + \tilde{E}^t_{0y}$$

$$\tilde{E}^r_{0xz} = -\tilde{E}^i_{0xz} + \frac{k_1}{k_2}\frac{\sqrt{k_2^2 - k_x^2}}{\sqrt{k_1^2 - k_x^2}}\,\tilde{E}^t_{0xz}$$

Since

$$\vec{E}^\alpha(x,z) = \int_{-\infty}^{\infty} \vec{\tilde{E}}^\alpha_0(k_x)\exp\left(i\left(k_x x + \sqrt{k^2 - k_x^2}\,z\right)\right)dk_x$$

If we know a complete electric field at $z = 0$ or $\vec{E}^\alpha(x,0)$

$$\vec{E}^\alpha(x,0) = \int_{-\infty}^{\infty}\vec{\tilde{E}}^\alpha_0(k_x)\exp(ik_x x)\,dk_x$$

$$\vec{\tilde{E}}^\alpha_0(k_x) = \frac{1}{2\pi}\int_{-\infty}^{\infty}\vec{E}^\alpha(x,0)\exp(-ik_x x)\,dx$$

then we also know the integrating kernels of electric fields $\vec{\tilde{E}}_0^{\alpha}(k_x)$ and when we know the integrating kernel the electric fields are known everywhere $\vec{E}^{\alpha}(x, z)$. To find the integrating kernels, let consider an inverse Fourier transform of the following barrier function. Let a be a constant

$$
\begin{aligned}
f(x) &= \begin{cases} 0 & |x| \geq l \\ a & |x| < l \end{cases} \\
\tilde{f}(s) &= \frac{a}{2\pi} \int_{-l}^{l} \exp(-ixs)\, dx \\
&= a\frac{\sin(ls)}{\pi s}
\end{aligned}
$$

and the inverse Fourier transform of a constant is Dirac delta function.

$$
\begin{aligned}
f(x) &= a \\
\tilde{f}(s) &= a\delta(s)
\end{aligned}
$$

These suggest that integrating kernels of the reflected wave $\vec{\tilde{E}}_0^r(k_x)$ and transmitted wave $\vec{\tilde{E}}_0^t(k_x)$ in equation (51) are

$$
\tilde{E}_{0x}^r(k_x) = \tilde{e}_{0xz}^i \frac{\sqrt{k_1^2 - k_{x0}^2}}{k_1} \left\{ -\delta(k_x - k_{x0}) - \left[\frac{2\frac{k_1}{k_2}\frac{\sqrt{k_2^2 - k_{x0}^2}}{\sqrt{k_1^2 - k_{x0}^2}}\sqrt{\frac{\epsilon_2\mu_2}{\epsilon_1\mu_1}}\sqrt{k_2^2 - k_{x0}^2}}{\frac{\epsilon_2}{\epsilon_1}\sqrt{k_1^2 - k_{x0}^2} + \sqrt{k_2^2 - k_{x0}^2}} \right] \frac{\sqrt{k_2^2 - k_{x0}^2}}{k_2}\frac{\sin(lk_x)}{\pi k_x} \right\}
$$

$$
\tilde{E}_{0y}^r(k_x) = \tilde{e}_{0y}^i \left\{ -\delta(k_x - k_{x0}) + \left[\frac{2\frac{\mu_2}{\mu_1}\sqrt{k_1^2 - k_{x0}^2}}{\frac{\mu_2}{\mu_1}\sqrt{k_1^2 - k_{x0}^2} + \sqrt{k_2^2 - k_{x0}^2}} \right] \frac{\sin(lk_x)}{\pi k_x} \right\}
$$

$$
\tilde{E}_{0z}^{r}(k_x) \;=\; \tilde{e}_{0xz}^{i}\frac{k_{x0}}{k_1}\Bigg\{ -\delta(k_x - k_{x0})
$$
$$
+\left[\frac{2\dfrac{k_1}{k_2}\dfrac{\sqrt{k_2^2-k_{x0}^2}}{\sqrt{k_1^2-k_{x0}^2}}\sqrt{\dfrac{\epsilon_2\mu_2}{\epsilon_1\mu_1}}\sqrt{k_2^2-k_{x0}^2}}{\dfrac{\epsilon_2}{\epsilon_1}\sqrt{k_1^2-k_{x0}^2}+\sqrt{k_2^2-k_{x0}^2}}\right]\frac{k_{x0}}{k_2}\frac{\sin(lk_x)}{\pi k_x}\Bigg\}
$$

$$
\tilde{E}_{0x}^{t}(k_x) \;=\; -\tilde{e}_{0xz}^{i}\frac{\sqrt{k_1^2-k_{x0}^2}}{k_1}\left[\frac{2\sqrt{\dfrac{\epsilon_2\mu_2}{\epsilon_1\mu_1}}\sqrt{k_2^2-k_{x0}^2}}{\sqrt{k_2^2-k_{x0}^2}+\dfrac{\epsilon_2}{\epsilon_1}\sqrt{k_1^2-k_{x0}^2}}\right]\frac{\sqrt{k_2^2-k_{x0}^2}}{k_2}\frac{\sin(lk_x)}{\pi k_x}
$$

$$
\tilde{E}_{0y}^{t}(k_x) \;=\; \tilde{e}_{0y}^{i}\left[\frac{2\dfrac{\mu_2}{\mu_1}\sqrt{k_1^2-k_{x0}^2}}{\sqrt{k_2^2-k_{x0}^2}+\dfrac{\mu_2}{\mu_1}\sqrt{k_1^2-k_{x0}^2}}\right]\frac{\sin(lk_x)}{\pi k_x}
$$

$$
\tilde{E}_{0z}^{t}(k_x) \;=\; \tilde{e}_{0xz}^{i}\frac{k_{x0}}{k_1}\left[\frac{2\sqrt{\dfrac{\epsilon_2\mu_2}{\epsilon_1\mu_1}}\sqrt{k_2^2-k_{x0}^2}}{\sqrt{k_2^2-k_{x0}^2}+\dfrac{\epsilon_2}{\epsilon_1}\sqrt{k_1^2-k_{x0}^2}}\right]\frac{k_{x0}}{k_2}\frac{\sin(lk_x)}{\pi k_x}
$$

Once we know the integrating kernels, we implicitly know the electric fields of the scattered waves

$$
E_x^{r}(x,z) \;=\; \tilde{e}_{0xz}^{i}\frac{\sqrt{k_1^2-k_{x0}^2}}{k_1}\Bigg\{ -\exp\!\left(i\left(k_{x0}x+\sqrt{k_1^2-k_{x0}^2}\,z\right)\right)
$$
$$
-\left[\frac{2\dfrac{k_1}{k_2}\dfrac{\sqrt{k_2^2-k_{x0}^2}}{\sqrt{k_1^2-k_{x0}^2}}\sqrt{\dfrac{\epsilon_2\mu_2}{\epsilon_1\mu_1}}\sqrt{k_2^2-k_{x0}^2}}{\dfrac{\epsilon_2}{\epsilon_1}\sqrt{k_1^2-k_{x0}^2}+\sqrt{k_2^2-k_{x0}^2}}\right]\frac{\sqrt{k_2^2-k_{x0}^2}}{k_2}
$$
$$
\times\int_{-\infty}^{\infty}\frac{\sin(lk_x)}{\pi k_x}\exp\!\left(i\left(k_x x+\sqrt{k_1^2-k_x^2}\,z\right)\right)dk_x\Bigg\}
$$

$$E_y^r(x,z) = \tilde{e}_{0y}^i \left\{ -\exp\left(i\left(k_{x0}x + \sqrt{k_1^2 - k_{x0}^2}\, z \right) \right) \right.$$

$$+ \left[\frac{2\frac{\mu_2}{\mu_1}\sqrt{k_1^2 - k_{x0}^2}}{\frac{\mu_2}{\mu_1}\sqrt{k_1^2 - k_{x0}^2} + \sqrt{k_2^2 - k_{x0}^2}} \right]$$

$$\left. \times \int_{-\infty}^{\infty} \frac{\sin(lk_x)}{\pi k_x}\exp\left(i\left(k_x x + \sqrt{k_1^2 - k_x^2}\, z \right) \right) dk_x \right\}$$

$$E_z^r(x,z) = \tilde{e}_{0xz}^i \frac{k_{x0}}{k_1} \left\{ -\exp\left(i\left(k_{x0}x + \sqrt{k_1^2 - k_{x0}^2}\, z \right) \right) \right.$$

$$+ \left[2\frac{k_1}{k_2}\frac{\sqrt{k_2^2 - k_{x0}^2}}{\sqrt{k_1^2 - k_{x0}^2}}\frac{\sqrt{\frac{\epsilon_2 \mu_2}{\epsilon_1 \mu_1}}\sqrt{k_2^2 - k_{x0}^2}}{\frac{\epsilon_2}{\epsilon_1}\sqrt{k_1^2 - k_{x0}^2} + \sqrt{k_2^2 - k_{x0}^2}} \right] \frac{k_{x0}}{k_2}$$

$$\left. \times \int_{-\infty}^{\infty} \frac{\sin(lk_x)}{\pi k_x}\exp\left(i\left(k_x x + \sqrt{k_1^2 - k_x^2}\, z \right) \right) dk_x \right\}$$

$$E_x^t(x,z) = \tilde{e}_{0xz}^i \frac{\sqrt{k_1^2 - k_{x0}^2}}{k_1} \left[\frac{2\sqrt{\frac{\epsilon_2 \mu_2}{\epsilon_1 \mu_1}}\sqrt{k_2^2 - k_{x0}^2}}{\frac{\epsilon_2}{\epsilon_1}\sqrt{k_1^2 - k_{x0}^2} + \sqrt{k_2^2 - k_{x0}^2}} \right] \frac{\sqrt{k_2^2 - k_{x0}^2}}{k_2}$$

$$\times \int_{-\infty}^{\infty} \frac{\sin(lk_x)}{\pi k_x}\exp\left(i\left(k_x x + \sqrt{k_2^2 - k_x^2}\, z \right) \right) dk_x$$

$$E_y^t(x,z) = \tilde{e}_{0y}^i \left[\frac{2\frac{\mu_2}{\mu_1}\sqrt{k_1^2 - k_{x0}^2}}{\frac{\mu_2}{\mu_1}\sqrt{k_1^2 - k_{x0}^2} + \sqrt{k_2^2 - k_{x0}^2}} \right]$$

$$\times \int_{-\infty}^{\infty} \frac{\sin(lk_x)}{\pi k_x}\exp\left(i\left(k_x x + \sqrt{k_2^2 - k_x^2}\, z \right) \right) dk_x$$

$$E_z^t(x,z) = \tilde{e}_{0xz}^i \frac{k_{x0}}{k_1} \left[\frac{2\sqrt{\frac{\epsilon_2 \mu_2}{\epsilon_1 \mu_1}}\sqrt{k_2^2 - k_{x0}^2}}{\frac{\epsilon_2}{\epsilon_1}\sqrt{k_1^2 - k_{x0}^2} + \sqrt{k_2^2 - k_{x0}^2}} \right] \frac{k_{x0}}{k_2}$$

$$\times \int_{-\infty}^{\infty} \frac{\sin(lk_x)}{\pi k_x}\exp\left(i\left(k_x x + \sqrt{k_2^2 - k_x^2}\, z \right) \right) dk_x$$

The scattered wave components can be concluded into vectors

$$\vec{E}^r(x,z) \quad = \quad \begin{aligned} &-\vec{E}^i(x,z) \\ &+ \xi(k_{x0})\vec{\tilde{E}}_0^t(k_{x0}) \\ &\times \int_{-\infty}^{\infty} \frac{\sin(lk_x)}{\pi k_x} \exp\left(i\left(k_x x \sqrt{k_1^2 - k_x^2}z\right)\right) dk_x \end{aligned} \qquad (53.1)$$

$$\vec{E}^t(x,z) \quad = \quad \vec{\tilde{E}}_0^t(k_{x0}) \int_{-\infty}^{\infty} \frac{\sin(lk_x)}{\pi k_x} \exp\left(i\left(k_x x + \sqrt{k_2^2 - k_x^2}z\right)\right) dk_x \qquad (53.2)$$

Where ξ is

$$\xi(k_x) \quad = \quad \begin{cases} 1 & \text{for } y \text{ component} \\ \dfrac{k_1}{k_2}\dfrac{\sqrt{k_2^2 - k_x^2}}{\sqrt{k_1^2 - k_x^2}} & \text{for } x \text{ and } z \text{ components} \end{cases}$$

Notice that the reflected electric field consists of the total reflection when there is no slit on the first term and slit effect on the second term which depends on the transmitted $\xi\vec{\tilde{E}}_0^t(k_{x0})$. Furthermore, equation (53.2) suggests that the transmitted wave is contributed from 2 parts, the first part is the transmission coefficient of the standard oblique incident wave scenarios and the slit integration part. Let's consider $\xi\vec{\tilde{E}}_0^t(k_{x0})$

$$\frac{k_1}{k_2}\frac{\sqrt{k_2^2 - k_{x0}^2}}{\sqrt{k_1^2 - k_{x0}^2}} \tilde{E}_{0xz}^t(k_{x0}) \quad = \quad \tilde{e}_{0xz}^i \left[\frac{2\dfrac{k_1}{k_2}\dfrac{\sqrt{k_2^2 - k_{x0}^2}}{\sqrt{k_1^2 - k_{x0}^2}}\sqrt{\dfrac{\epsilon_2\mu_2}{\epsilon_1\mu_1}}\sqrt{k_1^2 - k_{x0}^2}}{\dfrac{\epsilon_2}{\epsilon_1}\sqrt{k_1^2 - k_{x0}^2} + \sqrt{k_2^2 - k_{x0}^2}}\right]$$

$$\tilde{E}_{0y}^t(k_{x0}) \quad = \quad \tilde{e}_{0y}^i \left[\frac{2\dfrac{\mu_2}{\mu_1}\sqrt{k_1^2 - k_{x0}^2}}{\dfrac{\mu_2}{\mu_1}\sqrt{k_1^2 - k_{x0}^2} + \sqrt{k_2^2 - k_{x0}^2}}\right]$$

for the normal incident wave

$$\xi\tilde{E}_{0xz}^t(0) \quad = \quad \tilde{e}_{0xz}^i \left[\frac{2}{\sqrt{\dfrac{\epsilon_2\mu_1}{\epsilon_1\mu_2}} + 1}\right] \qquad (54.1)$$

$$\xi\tilde{E}_{0y}^t(0) \quad = \quad \tilde{e}_{0y}^i \left[\frac{2}{\sqrt{\dfrac{\epsilon_2\mu_1}{\epsilon_1\mu_2}} + 1}\right] \qquad (54.2)$$

For the case where wave propagates from a vacuum to a plasma

$$\sqrt{\frac{\epsilon_2 \mu_1}{\epsilon_1 \mu_2}} = \sqrt{1 - \frac{\omega_p^2}{\omega^2}}$$

Define dimensionless frequency $\widehat{\omega}$, the transmission coefficient in the reflected wave of y-component $t_{r,y}(\widehat{\omega})$ and the transmission coefficient in the reflected wave of xz-component $t_{r,xz}(\widehat{\omega})$.

$$\widehat{\omega} = \frac{\omega}{\omega_p}$$

$$t_{r,y}(\widehat{\omega}) = \frac{\xi \tilde{E}_{0y}^t(0)}{\tilde{e}_{0y}^i}$$

$$t_{r,xz}(\widehat{\omega}) = \frac{\xi \tilde{E}_{0xz}^t(0)}{\tilde{e}_{0xz}^i}$$

We have the dimensionless expression of $\xi \vec{\tilde{E}}_0^t(k_{x0})$ for the normal incident (54)

$$t_{r,\alpha}(\widehat{\omega}) = 2\widehat{\omega}^2 - 2\widehat{\omega}\sqrt{\widehat{\omega}^2 - 1} \qquad (55)$$

Equations (55) shows that $t_{r,\alpha}(\widehat{\omega})$ is complex when $\widehat{\omega} < 1$ and real when $\widehat{\omega} \geq 1$. This complex nature suggests a phase shift of scattered electric field at $z = 0$ causing the transmission coefficient to be greater than 1. The transmission coefficient and reflection coefficient at the slit is plotted in **Figure 28** and **Figure 29** respectively.
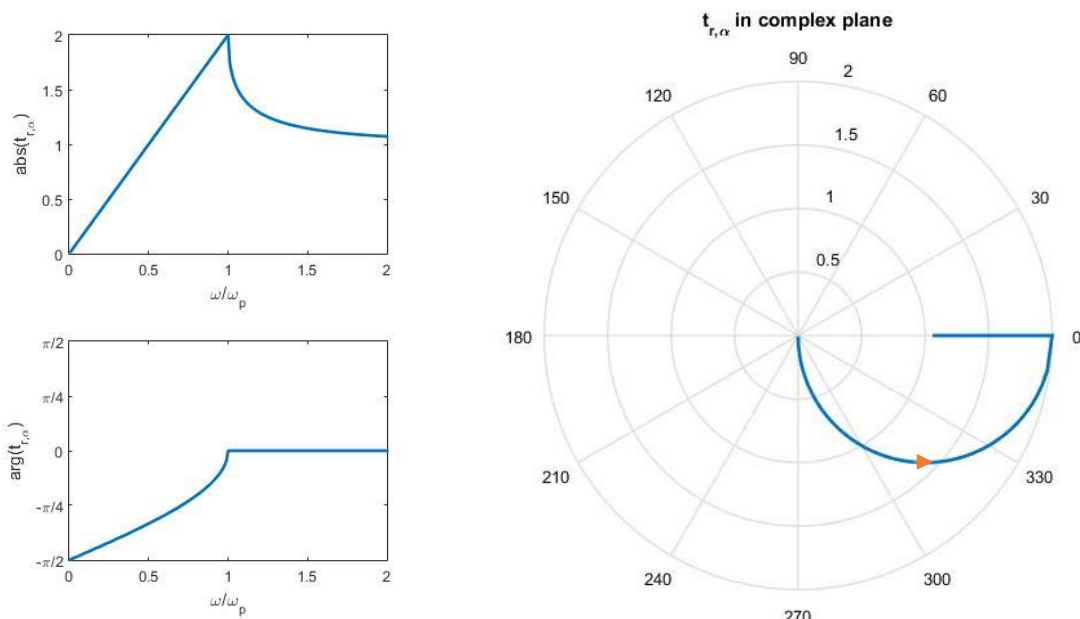

Figure 28 (left) The magnitude and argument of $t_{r,\alpha}(\omega)$, (right) $t_{r,\alpha}(\omega)$ plotted in the complex plane.
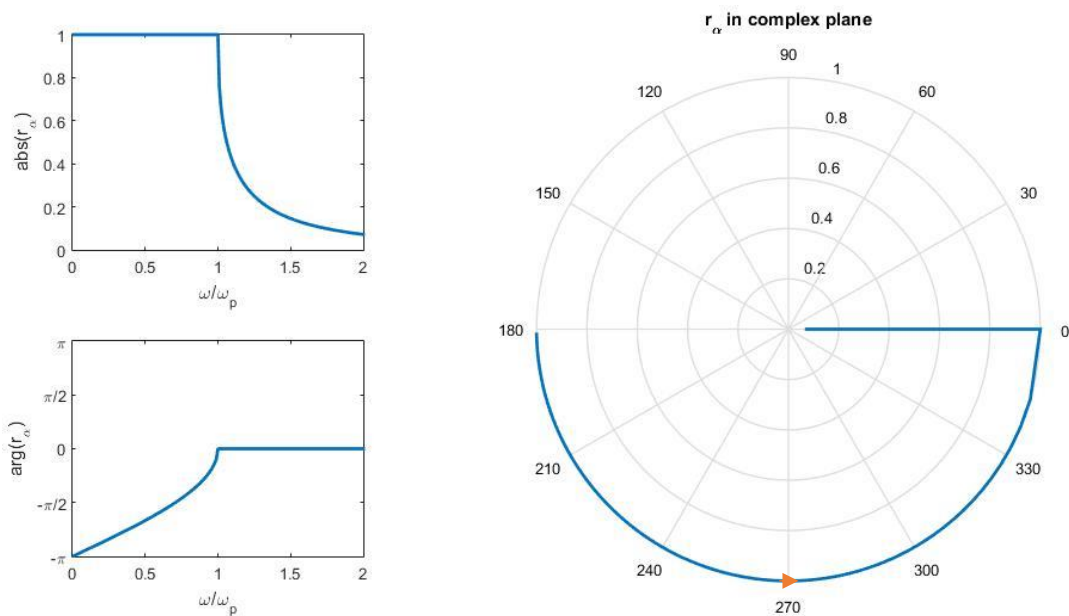

Figure 29 (left) The magnitude and argument of $r_\alpha(\omega)$, (right) $r_\alpha(\omega)$ plotted in the complex plane.

4.3 APPLICATION OF SLIT MODEL ON CURLING PROBE

To apply the single slit model for estimating the reflection coefficient of the curling probe. We consider the scenario where the normal incident wave without y-component of electric field scatters a single perfectly conducting slit to be model of TEM wave from a coaxial transmission line approaching the probe's slot as shown in **Figure 30**.
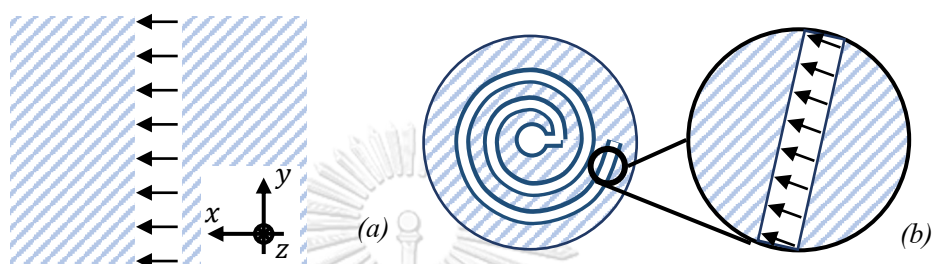

Figure 30 *The modeling of the curling probe as a plane single slit. (a) A single slit with normal incident wave without y-component of the electric field, (b) a curling probe with TEM field at an infinitesimal point on the slot.*

Assume that the reflected wave profile in the coaxial transmission line at the slot is the same as the single slit profile. The profile can be expanded into TEM, TE and TM modes of the transmission line. If the frequencies used to measure the reflection coefficient is not exceed the first cut off frequency of non-TEM mode, then the TE and TM compositions of the profile will dissipate along the transmission line leaving only TEM mode to reach the measurement apparatus. The TEM mode electric field of a single plane on a coaxial transmission line masks with $t_{r,xz}$ profile estimated from the single slit model is assumed to be the second part of the reflected electric field, equation (53.1), at the slot. Examples of the TEM mode electric field, $t_{r,xz}$ profile and their product of a coaxial transmission line with 0.2 core conductor radius and 2.31 shield conductor radius are shown in **Figure 31**, **Figure 32** and **Figure 33** respectively. **Figure 34** shows the cross-section of the second part of the reflected electric field at $\theta = 0$.
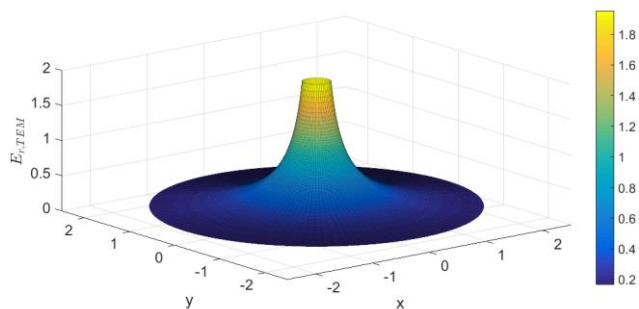
Figure 31 *An example of TEM mode radial electric field amplitude in a coaxial transmission*

line.

Figure 32 *An example of the transmission coefficient in the reflected wave of xz-component*

estimated on the curling probe slot using the single slit model.

จุฬาลงกรณ์มหาวิทยาลัย

CHULALONGKORN UNIVERSITY

Figure 33 *The second part of the reflected electric field, equation (53.1), at the slot as the*

product of TEM mode electric field and transmission coefficient in the reflected wave of xz

components
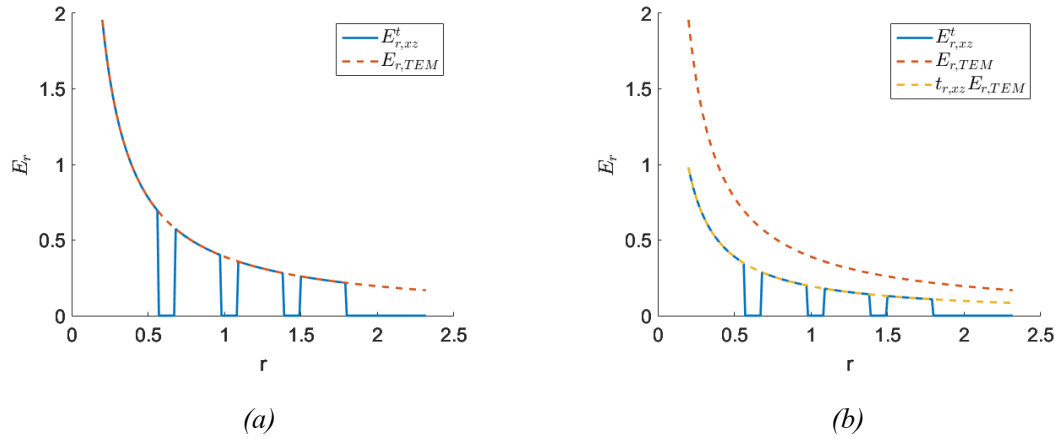
Figure 34 the cross-section of Figure 33 at $\theta = 0$ (a) when the incident wave frequency is lower than plasma frequency, (b) when the incident wave frequency is greater than plasma frequency.

If the second part of reflected electric field, equation (53.1), can be expanded into a series of TEM, TE and TM modes

Let

$$\int_{-\infty}^{\infty} \frac{\sin(lk_x)}{\pi k_x} \exp\left(i \left(k_x x + \sqrt{k_1^2 - k_x^2} z \right) \right) dk_x = \mathcal{I}$$
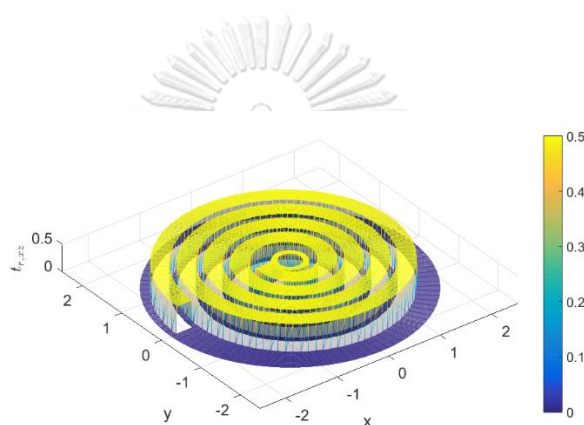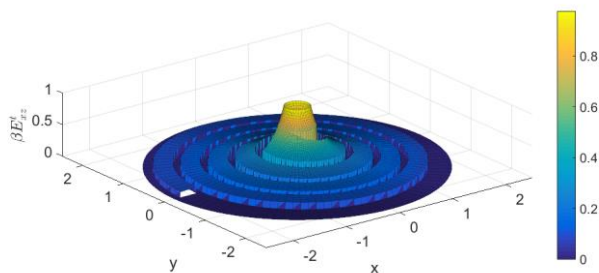
Then the second part of the reflected electric field is $\beta \vec{\tilde{E}}_0^t(k_{x0}) \mathcal{I}$.

$$\beta \vec{\tilde{E}}_0^t(k_{x0}) \mathcal{I} \;=\; t_{r,xz}(\omega) \left(a|TEM\rangle + \sum_i b_i \, |TE\rangle + \sum_i c_i |TM\rangle \right)$$

$$\vec{E}^i \;=\; |TEM\rangle$$

TE and TM modes of $\beta \vec{\tilde{E}}_0^t(k_{x0}) \mathcal{I}$ will dissipate when the wave propagates for some distance. The remaining of the reflected wave will be

$$\vec{E}^r \;=\; \left(-1 + a \cdot t_{r,xz}(\omega) \right) \vec{E}^i$$

Then the estimation of the reflection coefficient of the curling probe is

$$\Gamma(\omega) \quad = \quad -1 + a \cdot t_{r,xz}(\omega)$$

To determine the value of a, the extensive analysis of coaxial transmission line modes must be done. However, we know that a is somewhere between 0 and 1. **Figure 35** shows the magnitude, argument, and logarithm of the magnitude of the reflection coefficient of the curling probe for various a.

The results of the single slit model show that when $a < 0.5$ the curling probe matched frequency is the plasma frequency. When $a > 0.5$ the matched frequency increasing nonlinearly proportional to a and cannot be determined yet. However, the experiments did not agree with our proposed model.
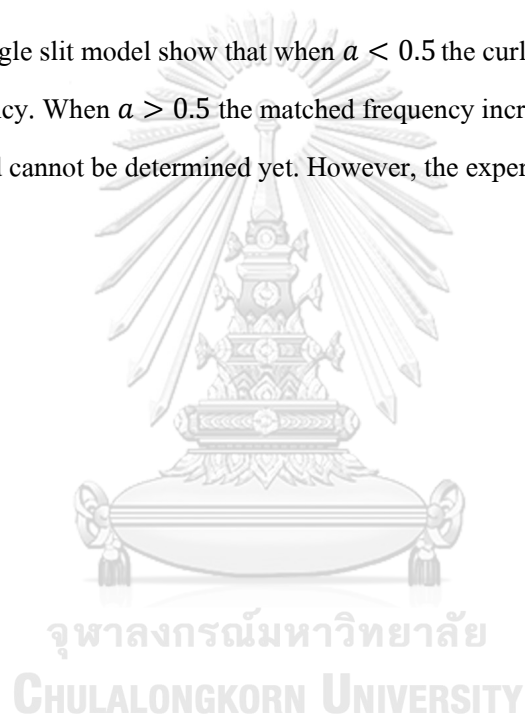
Figure 35 *The magnitude, argument, and logarithm of the magnitude of the reflection coefficient*

of a coaxial transmission line load with a curling probe estimated from the single slit model.

4.4 INVESTIGATION IN THE CURLING PROBE RESPONSES

In both our experiments and simulation in chapter III, when we measured the magnitude voltage reflection coefficient spectrum, there always was the minimum voltage reflection coefficient. According to the results reported in chapter III, the magnitude of the vol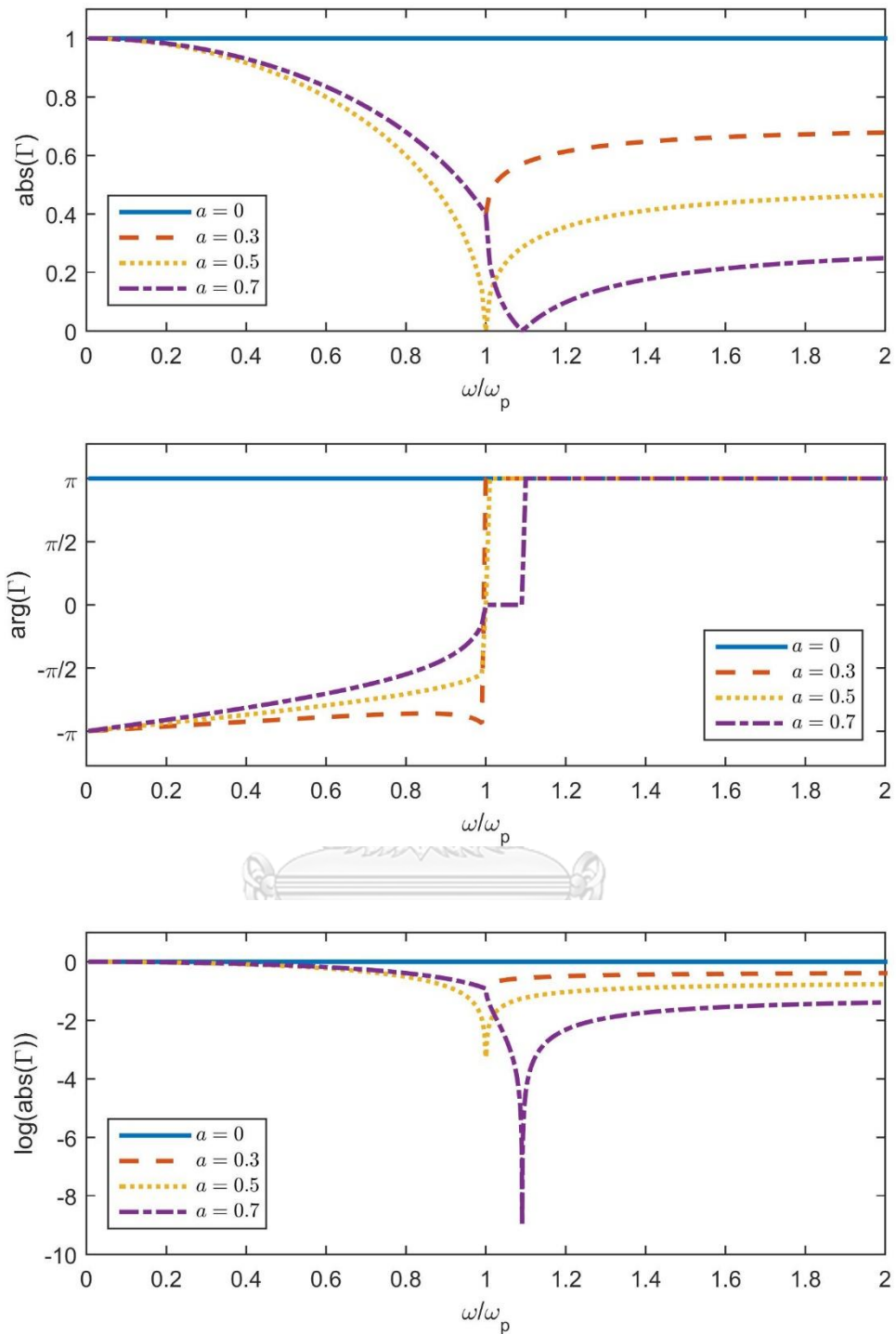tage reflection coefficient did not respond to the change of plasma density. However, the magnitude of the voltage reflection coefficient responded to the presence of other materials. We have performed both experiments and simulations when the curling probe faced different materials with different distances between the probe and the materials.

Figure 36 The experiment setup for investigating the probe voltage reflection coefficient spectrum responses.

4.4.1 EXPERIMENTS

The experiment setup is shown in **Figure 36**. The curling probe was fixed on top of the movable platform where materials would be placed, the distances between the probe and the materials were measured by a ruler held by modeling clay. The setup was carefully leveled by a bubble level. The reference position was the position where the materials in contact with the probe which was different for each material due to their thickness.

The materials, we used in the experiments, were composite epoxy FR-4 used in circuit broad, glass, plastic, paper, and copper. The surface of the materials was flat, the thickness of each material was not equal and shown in **Table 2**. The thickness of the epoxy and glass were measured by a vernier caliper while those of the paper, plastic, and copper were measured by a micrometer.
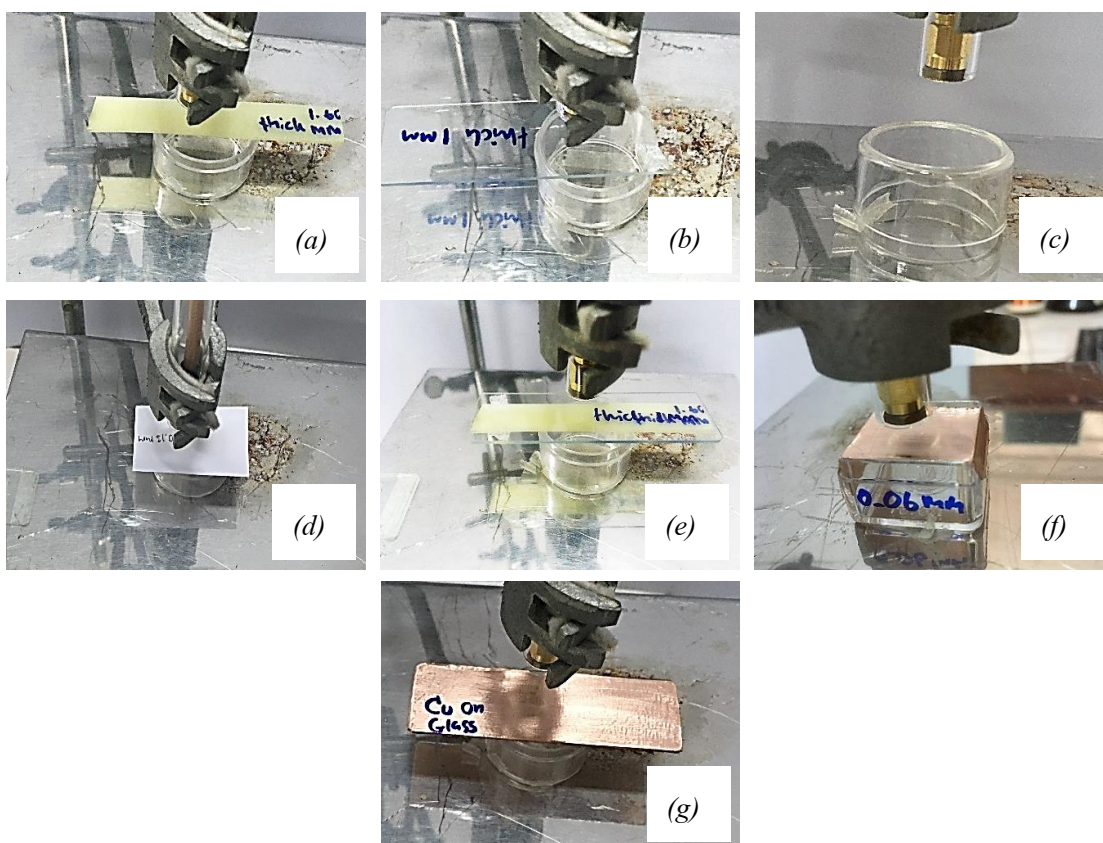

Figure 37 *The pictures shows how each material was placed on the platform (a) epoxy, (b) glass, (c) plastic, (d) paper, (e) glass stacked on epoxy, (f) copper, and (g) copper stacked on the glass.*

Material	Thickness (mm)
Epoxy	1.60
Glass	1.00
Paper	0.13
Plastic	0.83
Copper	0.06

Table 2 The thickness of each material used in the experiments

The experiments were performed on each material, the glass stacked on top of the epoxy and the copper stacked on top of the glass. The setups for each experiment are shown in **Figure 37**. The voltage reflection coefficient spectrum was measured for the distance between the probe and materials are 0mm to 10mm with 1mm for each step since the best resolution of the ruler is 1mm. The matched frequency shifted significantly when varied the position between 0mm and 1mm. in the case where the probe directly contacted the copper, there was no matched frequency, or the incident wave totally reflected on the entire spectrum. The minimum of voltage reflection coefficient spectrum appeared again when the copper was parted from the probe. The voltage reflection coefficient spectrum of epoxy and copper are shown in **Figure 38**, the rest are presented in appendix A4 and the matched frequency responded to the change of the distance is shown in **Figure 39**.

Figure 38 The voltage reflection coefficient spectrums over the frequency range between 1GHz and 8.5 GHz measured in experiments for each position (left) of epoxy, (right) of copper.

Figure 39 *The matched frequency responses to the position of each material from experiments.*

4.4.2 SIMULATIONS

The simulations of our constructed curling probe facing different materials were performed to ensure that the simulations showed the same trend as the experiments. The probe configuration is the same as the constructed probe configurations in subsection 3.2.2, the materials were modeled as a rectangular prism, the prism base was a square with 50mm side. The simulation configuration is shown in **Figure 40**.

The material properties such as permittivity, permeability, and electric conductivity were predefined by the CST microwave studio environment. The materials used for simulations were FR-4 as epoxy, mica as glass, paper, and copper. **Table 3** shows the physical properties of materials used in the simulations. The reference position of material is the curling probe face, the simulation simulated the voltage reflection coefficient for each position between 0mm to 10mm with 1mm step.
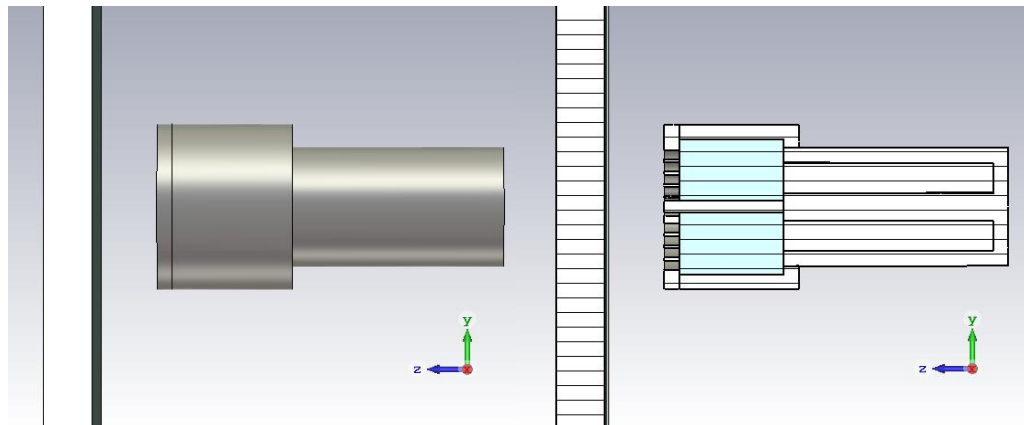
Figure 40 *(left) The configuration for the simulations of the probe facing different materials,*

(right) the cross-section in the x-axis of the configuration.

Material	Relative Permittivity	Relative Permeability	Electric Conductivity $(\Omega^{-1}m^{-1})$	Thickness (mm)
FR-4 (Epoxy)	4.3	1	0	1.6
Mica (Glass)	6.7	1	1×10^{-12}	1.0
Paper	2.31	1	0	0.13
Copper	n/a	1	5.8×10^{7}	0.06

Table 3 *The physical properties of each material used in simulations*

The simulated voltage reflection coefficient spectrums of epoxy and copper are shown in **Figure 41** while the rest are presented in appendix A4. The matched frequency significantly shifted when positions changed from 0mm to 1mm. In the case of copper, the voltage reflection coefficients, when the copper was in contact with the probe, were approximately 0 for the entire spectrum and reappears when the copper was parted from the probe face. The matched frequency when the position of the material changed is plotted in **Figure 42**.
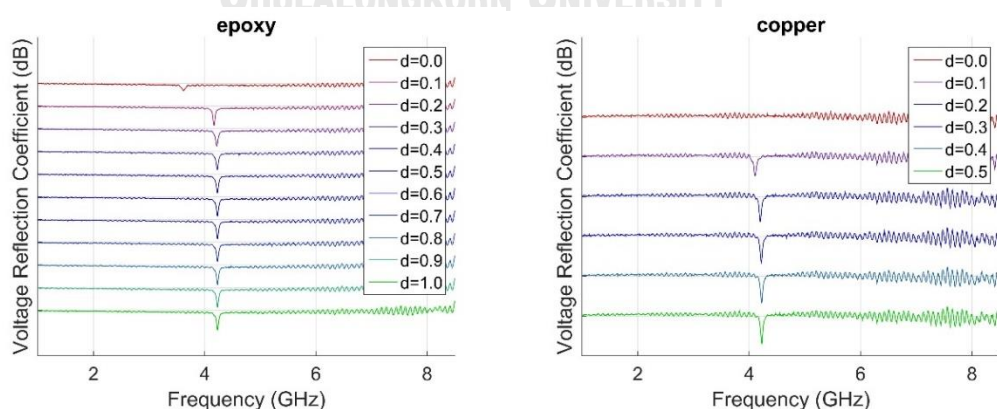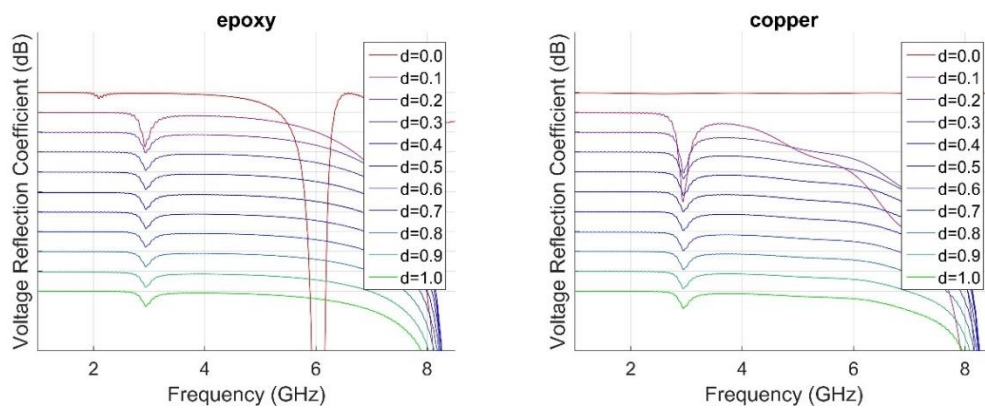
Figure 41 *The simulated voltage reflection coefficient spectrums over the frequency range between 1GHz and 8.5 GHz for each position (left) of epoxy, (right) of copper.*
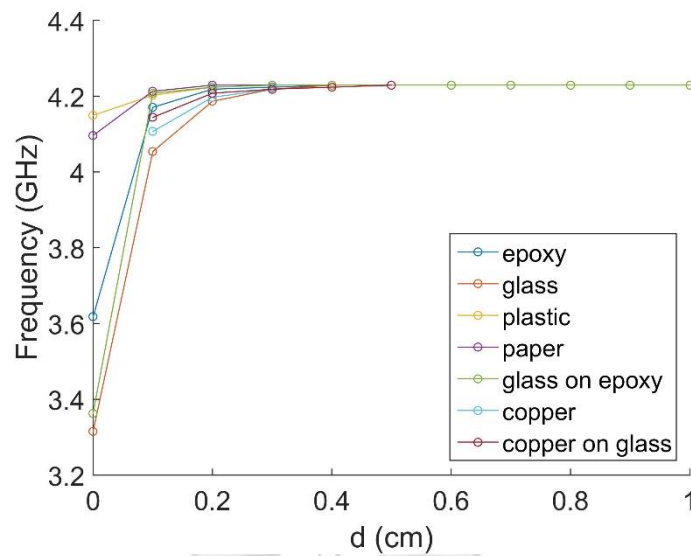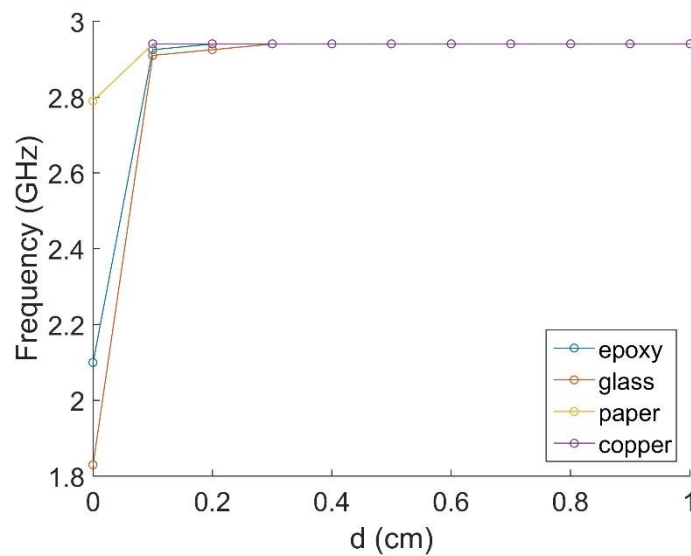

Figure 42 *The matched frequency responses to the position of each material from simulations*

Both experiments and simulations suggested the same, the matched frequency does respond to the presence of material in front of the probe and the results of both methods were agreed upon trend but the exact values. The matched frequencies predicted from the simulations were lower. The matched frequencies when the probe in contact with materials are increasing inversely proportional to the material permittivity, for instance, the matched frequency of the glass is less than those of the epoxy followed by those of the paper. However, the claim cannot be concluded since the thickness was not controlled. We found that when the probe faced a conductor, the

probe minimum voltage reflection coefficient disappears. It reappeared when the material was parted from the probe.

4.5 INVESTIGATION IN THE SLOT EFFECT ON THE VOLTAGE REFLECTION COEFFICIENT SPECTRUM

To investigate whether the slot affected the voltage reflection coefficient, we simulated 2 scenarios including the probe covered with perfectly conducting disk and the probe with the face replaced with a blank perfectly conducting disk as shown in **Figure 43** and **Figure 44** respectively. The simulated voltage reflection coefficient spectrums of both scenarios suggest that the minimum of reflection coefficient spectrum did not originate from the slot since both spectrums were nearly identical and did not has a minimum as shown in the result **Figure 45**.
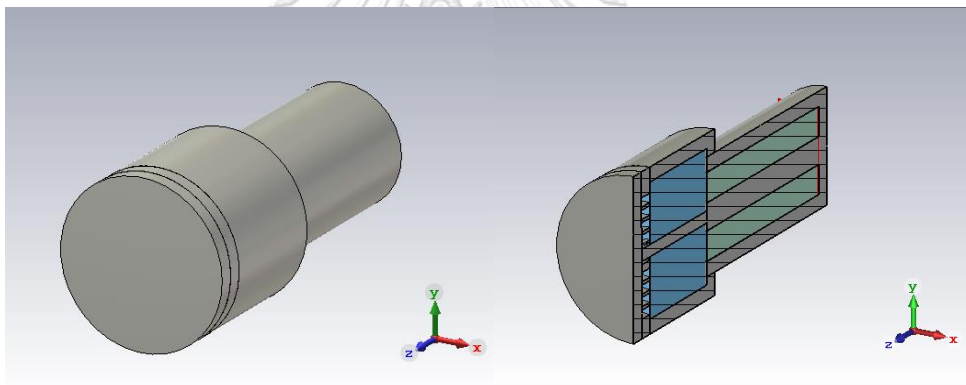
Figure 43 The configuration when perfectly conducting disk covered the slot
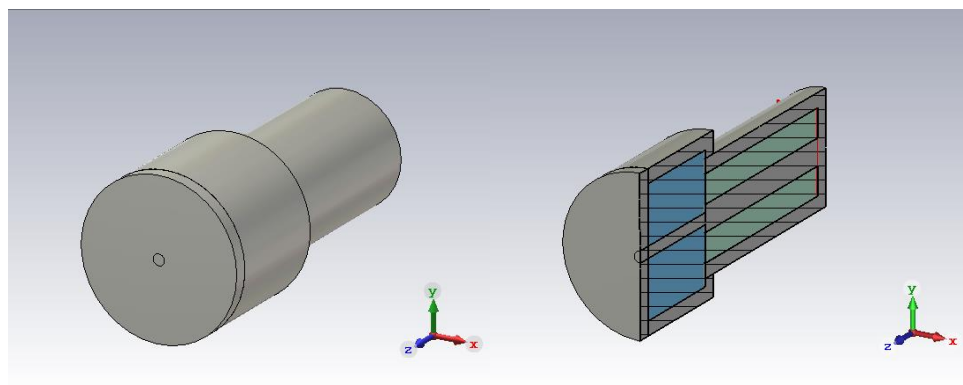
Figure 44 the configuration when the face of the curling probe was replaced with perfectly conducting blank disk
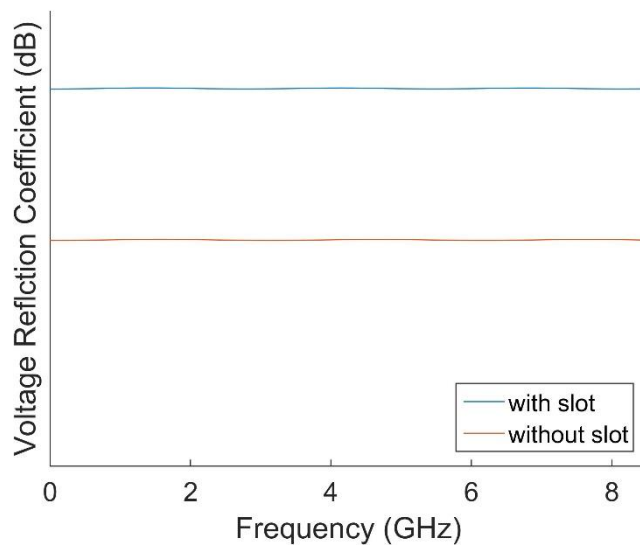
Figure 45 *The voltage reflection coefficient spectrum of the probe covered with perfectly*

conducting disk and the probe with the face replaced with a blank disk.

The first scenario can also be approximated as the probe touched a copper sheet. We can now compare the first scenario with the experiment where the probe directly touched the copper. The spectrum also did not show the distinguishable minimum which agreed with the simulated results.
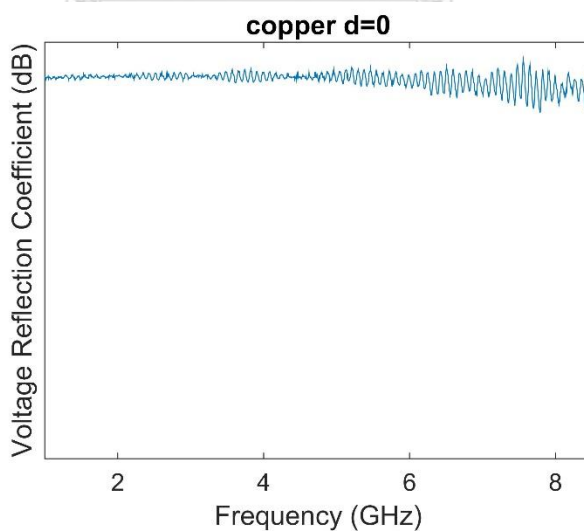
Figure 46 *The voltage reflection coefficient spectrum measured when the probe directly touched*

a copper.

According to the results, we can safely say that the slot itself was not the source of the minimum in the voltage reflection coefficient spectrum. This does not imply that the geometry of the slot does not affect the voltage reflection coefficient spectrum when the probe in contact with other mediums.

V CONCLUSIONS

The experiments of the constructed curling probe did not indicate any significant change in the matched frequency when the probe immersed in plasmas with different densities up to the maximum range of our network analyzer. Because there was no significant change, the plasma density cannot be measured. The objective that we would compare the measurement results between probes cannot be done. This led us to perform the simulations imitating the reported article [11], the simulation configuration included both the configuration reported in the article Figure 18 and our constructed probe configuration **Figure 22**. The simulated results showed that the reported configuration matched frequency does not respond to the change of plasma density as well as our constructed probe configuration which conformed to our experiments. This concluded that the proposed model in Liang [11] cannot be applied in our experiments and simulations. We have checked the assumptions of the models and found that the hairpin probe principles [7] from which the curling probe model was modified interpreted the matched frequency as the resonance frequency. The matched frequency is the frequency where the load impedance is equal to the characteristic impedance of the transmission line while the resonance frequency is the frequency when the load is vanished or infinite. The matched frequency can be detected by the minimum in voltage reflection coefficient spectrum and both frequencies are not allowed to be the same, this led us to remodel the probe from the ground up.

The idea used in the remodeling attained from Arshadi's work [13] which model the probe as a single slit and using vector potentials to solve Maxwell's equations to predict the resonance frequency. Instead of using vector potentials to determine the resonance frequency, we started from the electromagnetic fields itself to determine the reflected wave amplitudes and then we used the reflected wave amplitudes to estimate the voltage reflection coefficient spectrum. we chose to start from fields because the slot is a boundary value problem. The vector potentials are perfect when sources are considered, but for the boundary value problem, fields are preferred. Our probe model also suggested that the probe matched frequency should respond to the change of plasma density and have no minimum in the voltage reflection coefficient spectrum at all when the probe was immersed in a non-dispersive medium. This does not conform with our experiments since there always was a minimum in the voltage reflection coefficient spectrum

even if the probe was placed in a non-dispersive medium such as vacuum, referred to **Figure 17**. However, the model was excessively simplified and needs improvements.

Because the probe was not directly exposed to the plasma but covered with Pyrex glass and we also found that the probe responded to the presence of other materials placed in front of the probe as shown in **Figure 36**. Thus, we further investigated the probe reflection spectrum responding to other materials and the distance between material and the probe. We found that probe matched frequency shifted lower when the probe directly faced different materials and the matched frequency when directly faced with materials were increasing inversely proportional to the material's permittivity, however, the statements cannot be implied since we did not control the material thickness. Also, the probe reflection spectrum responded sensitively when the distance between the probe and materials were varied between 0mm and 1mm. Due to the limitation of our equipment, the precise measurement in the distance range cannot be performed.

We also would like to confirm that the minimum in the reflection spectrum is not excited by the slot alone but the result of the slot and mediums in front of it. The simulations when the probe face was covered by perfectly conducting disk and when the probe face was replaced by the perfectly conducting disk were performed. Both configurations are shown in **Figure 43** and **Figure 44** respectively. We found that both configurations gave nearly the same reflection spectrums, and there is no minimum in both spectrums, referred to **Figure 45**. This concluded that the minimum in reflection coefficient was not excited by not only the slot but also the medium in front of it.

VI FUTURE STUDY SUGGESTIONS

The probe was not only sensitive to the other materials but also any contact with the transmission line. The minimum in voltage reflection coefficient spectrum of the probe changed drastically when lightly touched the coaxial transmission line. We hypothesized that this might be the result of not properly calibrating the network analyzer since there was no calibration-kit in our possession. However, we try fixed the setup as much as possible to make the result consistence. Each experiment should be performed several times to determine the error bar which is used to indicate whether the change is random or actual change.

The plasmas generated in the experiments were not stable, they were ready to arc whenever there was an electrode between the chamber which, in this case, was our probe. Arcing release a large amount of current at once since we could not guarantee that our measurement tools can handle that kind of inrush current, the experiment when directly exposed the probe to the plasma has not been done. The more stable plasma generating setup is needed to directly expose the probe to the plasma.

Even though our proposed model cannot be applied to the curling probe experiments and simulations, we hypothesized that our proposed model prediction could be improved by solving the problem entirely in the cylindrical coordinate which we can include the coaxial transmission line and spiral slot to directly predict the voltage reflection coefficient spectrum.

Since we could not confidently say that the change in the minimum of voltage reflection coefficient spectrum is not significant and the change between experiments 1 and 2 in **Table 1** did fit the previously proposed model in which the matched frequency would increase directly proportional to the plasma density. The predicted density according to the equation (32) when δ equal to 1 is

$$n_e \quad = \quad \frac{2}{3.14 \times 10^{-4}}(f_1^2 - f_0^2) \qquad\qquad m^{-3}$$

The plasma density measured by the curling probe in experiment 2 was 2.83×10^{20} m^{-3} or 2.83×10^{14} cm^{-3} which is unexpectedly high for the plasma generated by the power approximately 7 W. if the results were reproducible, the probe may respond to the plasma density changes in the

power ranges. Intensive exploration in the range of power between 0 – 7 W generating power should be done.

The experiment setup used in the experiments was not reliable and not flexible and should be improved. When plasma was ignited and reignited with the same conditions the measured parameters are different. The problems we could identify were that the plasma chamber was leaking, the pressure gauge was not regularly calibrated, the glass part of the chamber and the argon gas feed system was not proper. The chamber leaking can be identified by that the vacuum pump cannot evacuate the chamber to the ultimate vacuum and the gas feeding system should be using the stainless steel tubes instead of Teflon tubes to reduce the leaking at the fitting which designed for fitting the stainless steel tube. The glass part does not have the ledges at the end causing the tight seal impossible. A larger chamber and homogeneous plasma generating setups are needed for researching plasma diagnostics. The good chamber must be able to reproduce the measurements.

In our experiments, there was only one slot for a diagnostic tool, however, the well-developed Langmuir probe should be used to exactly determine plasma density rather than using the power to indicate density changes.

APPENDICES

A1 VOLTAGE REFLECTION COEFFICIENT SIMPLE MEASUREMENT

To measure the reflection coefficient we do not need to directly measure the exact waveform of the voltage, only the standing wave ratio or SWR is required. The standing wave ratio is constant along a transmission line which much easier to detect than the exact waveform of the voltage. The standing wave ratio is the ratio between the maximum voltage and minimum voltage amplitudes on a transmission line. Using equation (3), the amplitude of the voltage in a transmission line is

$$|V(z)| \quad = \quad |V_0^+||1 + |\Gamma|\exp(i\theta - i2\beta z)|$$

where θ is the phase of the reflection coefficient. Since $-1 < \exp(i\theta - i2\beta z) < 1$

$$SWR \quad = \quad \frac{1 + |\Gamma|}{1 - |\Gamma|}$$

$$|\Gamma| \quad = \quad \frac{SWR - 1}{SWR + 1}$$

Let the first minimum amplitude occurs at $z = -l_{min}$ then $\theta + 2\beta l_{min} = \pi$. The phase of the reflection coefficient can now be determined.

$$\theta \quad = \quad \pi - 2\beta l_{min}$$

A2 THE RANGE OF VOLTAGE REFLECTION COEFFICIENT OF A PASSIVE LOAD

In this section, we will find that the magnitude of the voltage reflection coefficient of a passive load will be in the range of 0 to 1 and only equal to 1 when the load impedance is purely imaginary. Let us first consider the general voltage reflection coefficient (26)

$$\Gamma(Z_L) \quad = \quad \frac{Z_L - Z_0}{Z_L + Z_0}$$

Let $x = Z_L/Z_0$ as dimensionless impedance

$$\Gamma(x) \quad = \quad \frac{x-1}{x+1}$$

$x = x_R + ix_I$ is a complex number where $x_R \in \mathbb{R}^+ \cup \{0\}$ and $x_I \in \mathbb{R}$.

Considering the case when $x_R \in \mathbb{R}^+$

$$\Gamma(x) \quad = \quad \frac{(x_R - 1) + ix_I}{(x_R + 1) + ix_I}$$

$$|\Gamma(x)| \quad = \quad \frac{(x_R^2 + x_I^2 + 1) - 2x_R}{(x_R^2 + x_I^2 + 1) + 2x_R}$$

$$\arg(\Gamma(x)) \quad = \quad \arctan\left(\frac{2x_I}{x_R^2 + x_I^2 - 1}\right)$$

To determine the range of magnitude of voltage reflection coefficient, let $y = \frac{x_R^2 + x_I^2 + 1}{2x_R}$

$$|\Gamma(x)| \quad = \quad \frac{y-1}{y+1}$$

Find the range of y

$$y \quad = \quad \frac{x_R^2 + 1}{2x_R} + \frac{x_I^2}{2x_R}$$

Consider only the first term, we found that $\frac{x_R^2 + 1}{2x_R} > 0$. We find the minimum of the expression

$$\frac{d}{dx_R} \frac{x_R^2 + 1}{2x_R} \quad = \quad 0$$

$$1 - \frac{1}{x_R^2} \quad = \quad 0$$

$$x_R \quad = \quad 1$$

We found that $\frac{x_R^2 + 1}{2x_R} \geq 1$ and since $\frac{x_I^2}{2x_R} > 0$ then $y \geq 1$. The result implied that $|\Gamma(x)| \in [0,1)$ when $x_R \in \mathbb{R}^+$ and $x_I \in \mathbb{R}$. Next, let consider the case when $x_R = 0$, the magnitude and argument of voltage reflection coefficient are

$$|\Gamma(x)| \quad = \quad \frac{x_I^2 + 1}{x_I^2 + 1}$$

$$|\Gamma(x)| \quad = \quad 1$$

$$\arg(\Gamma(x)) \quad = \quad \arctan\left(\frac{2x_I}{x_I^2 - 1}\right)$$

The $|\Gamma(x)|$ always equal to 1 regardless of the reactance of the load.

A2.1 THE VOLTAGE REFLECTION COEFFICIENT OF A TRANSMISSION LINE RESONATOR

According to the transmission line resonator impedance (2727), the impedances for both cases of resonances are purely imaginary. This implied that the magnitude and argument of the voltage reflection coefficient cannot be used to detect the resonance frequencies of a transmission line resonator, but the argument might. The magnitude of the voltage reflection coefficient is used for detecting the matched frequency where load impedance equal to the transmission line characteristic impedances, not the resonance frequency where the load impedance is zero.

A3 PLASMA PERMITIVITY DERIVATION

The permittivity of mediums was derived by the dipole moment induced by the propagation of an electromagnetic wave. When the electromagnetic wave propagates through the medium charge particles respond, however, electron respond much faster than the ion and that the reason why only electron motion was considered. the displacement of electrons caused by the electric field induced the dipole moments [18]. Consider the equation of motion of an electron

$$m\left[\frac{d^2}{dt^2}\vec{x} + \gamma\frac{d}{dt}\vec{x} + \omega_0^2\vec{x}\right] \quad = \quad -e\vec{E}(\vec{x}, t)$$

Assuming the electromagnetic wave is a harmonic field with the time factor $\exp(-i\omega t)$ the dipole moment of the electron is

$$\vec{p} \quad = \quad \frac{e^2}{m}\frac{\vec{E}}{(\omega_0^2 - \omega^2 - i\omega\gamma)}$$

The relative permittivity is

$$\frac{\epsilon(\omega)}{\epsilon_0} = 1 + \frac{ne^2}{\epsilon_0 m}\sum_j \frac{f_j}{\omega_j^2 - \omega^2 - i\omega\gamma_j}$$

Where n is molecules density with Z electrons per molecule, electrons in a molecule are partitioned with binding frequency ω_j and damping constant γ_j associated with the number of electrons in the partition f_j and thus

$$\sum_j f_j = Z$$

Consider the term of free electron or ionized electron in case of gas of permittivity, assuming that f_0 electrons are ionized.

$$\frac{\epsilon(\omega)}{\epsilon_0} = 1 + \frac{ne^2}{\epsilon_0 m}\sum_j \frac{f_j}{\omega_j^2 - \omega^2 - i\omega\gamma_j} - \frac{ne^2}{\epsilon_0 m}\frac{f_0}{(\omega^2 + i\omega\gamma_0)}$$

Let

$$\omega_p = \frac{ne^2}{\epsilon_0 m}$$

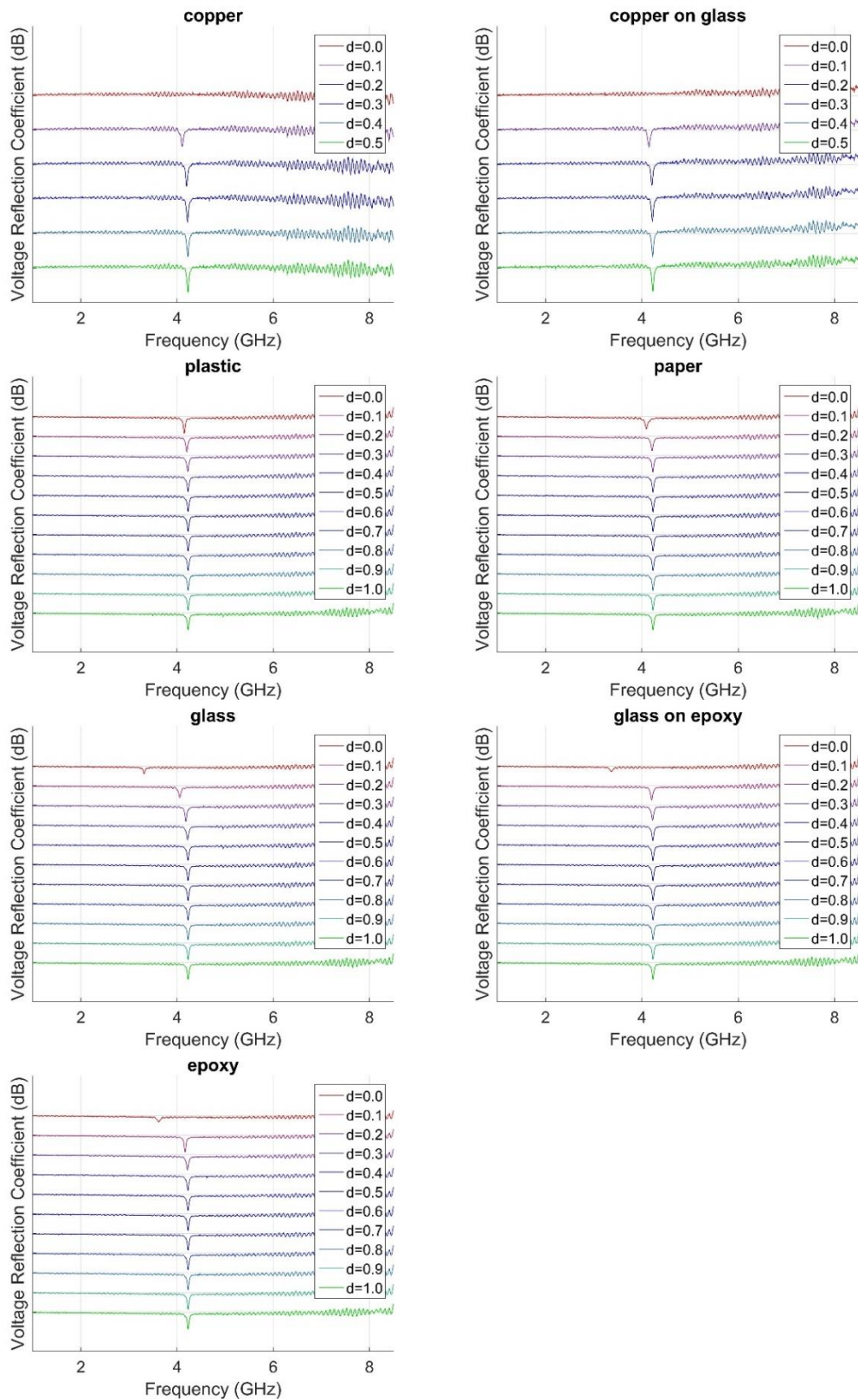For plasma, the bounding electron terms are neglected and $f_0 \approx 1$.

$$\frac{\epsilon(\omega)}{\epsilon_0} = 1 - \frac{\omega_p^2}{(\omega^2 + i\omega\gamma_0)}$$

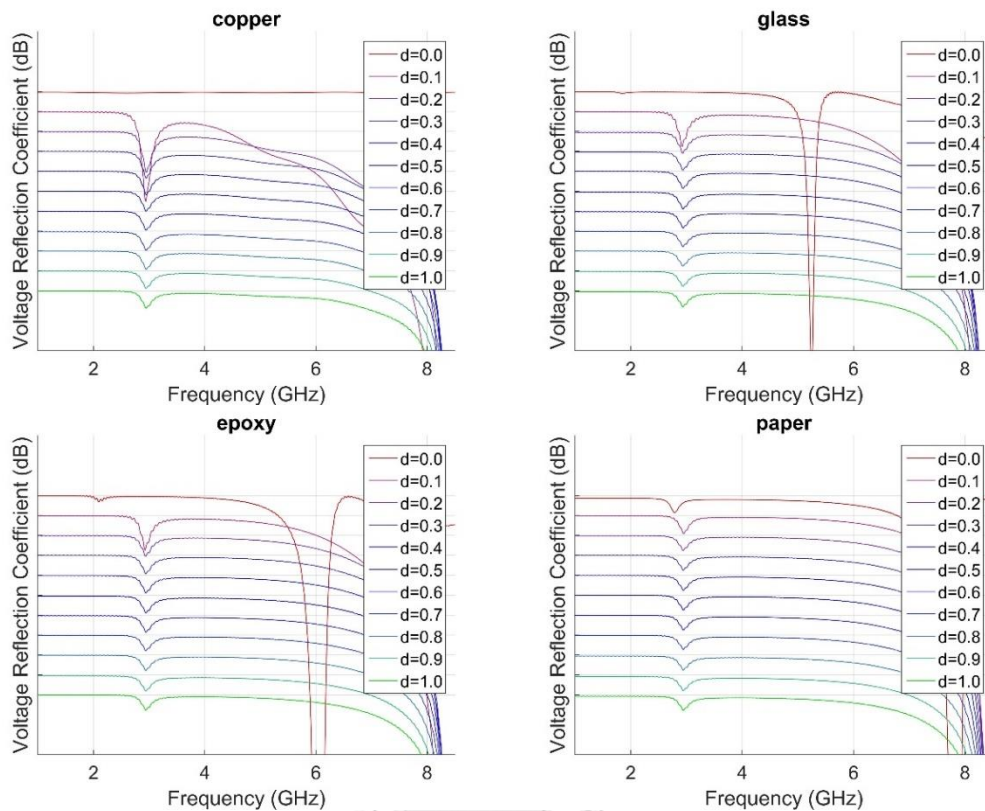Where ω_p is the plasma frequency, and for the high-frequency case

$$\frac{\epsilon(\omega)}{\epsilon_0} = 1 - \frac{\omega_p^2}{\omega^2}$$

A4 THE RESULTS FROM INVESTIGATION IN THE CURLING PROBE RESPONSES

A4.1 EXPERIMENTAL RESULTS

A4.2 SIMULATED RESULTS

A5 THE INCEASING PLASMA DENSITY PROPORTIONAL TO THE PLASMA GENERATING POWER EVIDENCES

We had performed density measurement by single Langmuir probe on another setup which the plasma did not arc, but the setup used the halfwave direct current voltage source rather than the constant direct current source. The results in **Figure 47** showed that the plasma density increase directly proportional to the discharge current. The plasma characteristic is almost ohmic in the setup thus, the discharge power was directly proportional to the discharge current.
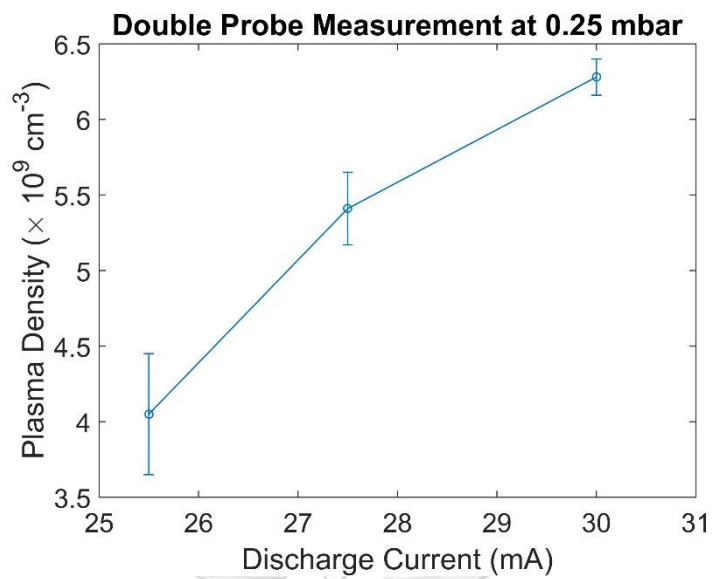
Figure 47 *The plasma density measurements using single Langmuir probe in different*

discharged currents

REFERENCES

1. Auciello O, Flamm DL. Plasma Diagnostics: Academics Press; 1989.

2. Chu PK, Lu X. Low Temperature Plasma Technology: Taylor & Francis; 2014.

3. Godyak VA, Demidov VI. Probe measurements of electron-energy distributions in plasmas: What can we measure and how can we achieve reliable results? Journal of Physics D: Applied Physics. 2011;44(23).

4. Fantz U. Basics of plasma spectroscopy. Plasma Sources Science and Technology. 2006;15(4):S137-S47.

5. Stenzel RL. Microwave resonator probe for localized density measurements in weakly magnetized plasmas. Review of Scientific Instruments. 1976;47(5):603-7.

6. Kondrat'ev IG, Kostrov AV, Smirnov AI, Strikovskiǐ AV, Shashurin AV. Two-wire microwave resonator probe. Plasma Physics Reports. 2002;28(11):900-5.

7. Piejak RB, Godyak VA, Garner R, Alexandrovich BM, Sternberg N. The hairpin resonator: A plasma density measuring technique revisited. Journal of Applied Physics. 2004;95(7):3785-91.

8. Lapke M, Mussenbrock T, Brinkmann RP. The multipole resonance probe: A concept for simultaneous determination of plasma density, electron temperature, and collision rate in low-pressure plasmas. Applied Physics Letters. 2008;93(5).

9. Lapke M, Oberrath J, Schulz C, Storch R, Styrnoll T, Zietz C, et al. The multipole resonance probe: Characterization of a prototype. Plasma Sources Science and Technology. 2011;20(4).

10. Oberrath J, Brinkmann RP. Active plasma resonance spectroscopy: Eigenfunction solutions in spherical geometry. Plasma Sources Science and Technology. 2014;23(6).

11. Liang I, Nakamura K, Sugai H. Modeling microwave resonance of curling probe for density measurements in reactive plasmas. Applied Physics Express. 2011;4(6).

12. Pandey A, Sakakibara W, Matsuoka H, Nakamura K, Sugai H. Curling probe measurement of electron density in pulse-modulated plasma. Applied Physics Letters. 2014;104(2).

13. Arshadi A, Peter Brinkmann R. Analytical investigation into the resonance frequencies of a curling probe. Plasma Sources Science and Technology. 2016;25(4).

14.   Lapke M, Oberrath J, Mussenbrock T, Brinkmann RP. Active plasma resonance spectroscopy: A functional analytic description. Plasma Sources Science and Technology. 2013;22(2).

15.   CST Microwave Studio: Work Flow and Solver Overview: CST GmbH–Computer Simulation Technology; 2008.

16.   Arshadi A, Brinkmann RP. Analytical investigation of microwave resonances of a curling probe for low and high-pressure plasma diagnostics. Plasma Sources Science and Technology. 2017;26(1).

17.   Clemmow PC. The Plane Wave Spectrum Representation of Electromagnetic Fields 2nd ed: Oxford University Press, USA/IEEE Press; 1996.

18.   Jackson JD. Classical Electrodynamics. 3rd ed: John Wiley & Sons; 1999.
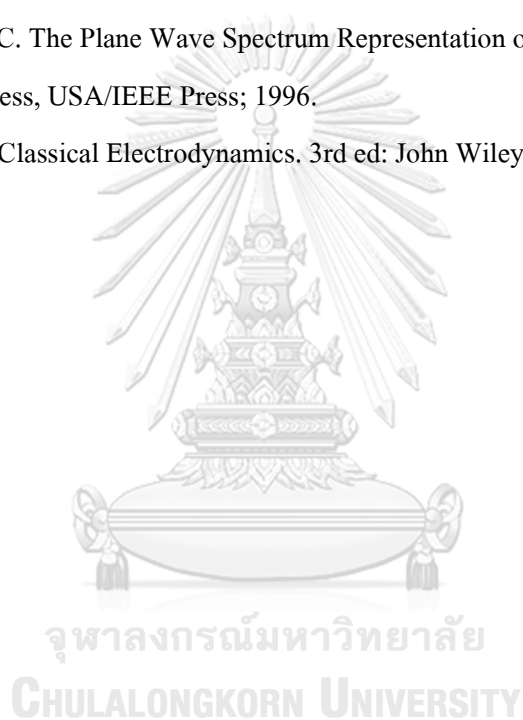
VITA

NAME   Chatchai Sirithipvanich

DATE OF BIRTH   27 March 1994

PLACE OF BIRTH   Bangkok, Thailand

INSTITUTIONS ATTENDED Chulalongkorn University

HOME ADDRESS   18/250 Siphraya Road, Mahapruktharam District, Bangrak,

                                        Bangkok 10500